

koopmans: an open-source package for accurately and efficiently predicting spectral properties with Koopmans functionals

Edward Linscott,^{*,†,@} Nicola Colonna,^{‡,¶,@} Riccardo De Gennaro,[†] Ngoc Linh Nguyen,^{§,||} Giovanni Borghi,^{†,△} Andrea Ferretti,[⊥] Ismaila Dabo,[#] and Nicola Marzari^{*,†,¶}

[†]*Theory and Simulation of Materials (THEOS), École Polytechnique Fédérale de Lausanne, 1015 Lausanne, Switzerland*

[‡]*Laboratory for Neutron Scattering and Imaging, Paul Scherrer Institut, 5232 Villigen, Switzerland*

[¶]*National Centre for Computational Design and Discovery of Novel Materials (MARVEL), École Polytechnique Fédérale de Lausanne, 1015 Lausanne, Switzerland*

[§]*Faculty of Materials Science and Engineering, Phenikaa University, Hanoi 12116, Vietnam*

^{||}*Phenikaa Research and Technology Institute (PRATI), A&A Green Phoenix Group JSC, No. 167 Hoang Ngan, Trung Hoa, Cau Giay, Hanoi 11313, Vietnam*

[⊥]*Centro S3, CNR-Istituto Nanoscienze, 41125 Modena, Italy*

[#]*Department of Materials Science and Engineering, Materials Research Institute, and Institutes of Energy and the Environment, The Pennsylvania State University, University Park, Pennsylvania 16802, USA*

[@]*Contributed equally to this work*

[△]*Now at Liceo Manfredo Fanti, 41012 Carpi, Italy*

E-mail: edward.linscott@epfl.ch; nicola.marzari@epfl.ch

Abstract

Over the past decade we have developed Koopmans functionals, a computationally efficient approach for predicting spectral properties with an orbital-density-dependent functional formulation. These functionals address two fundamental issues with density functional theory (DFT). First, while Kohn-Sham eigenvalues can loosely mirror experimental quasiparticle energies, they are not meant to reproduce excitation energies and there is formally no connection between the two (except for the HOMO for the exact functional). Second, (semi-)local DFT deviates from the expected piecewise linear behavior of the energy as a function of the total number of electrons. This can make eigenvalues an even poorer proxy for quasiparticle energies and, together with the absence of the exchange-correlation derivative discontinuity, contributes to DFT's underestimation of band gaps. By enforcing a generalized piecewise linearity condition to the entire electronic manifold, Koopmans functionals yield molecular orbital energies and solid-state band structures with comparable accuracy to many-body perturbation theory but at greatly reduced computational cost and preserving a functional formulation. This paper introduces `koopmans`, an open-source package that contains all of the code and workflows needed to perform Koopmans functional calculations without requiring expert knowledge. The theory and algorithms behind Koopmans functionals are summarized, and it is shown how one can easily use the `koopmans` package to obtain reliable spectral properties of molecules and materials.

How can one accurately and efficiently predict spectral properties of molecules and materials *ab initio*? Currently, the most accurate and popular approaches to compute charged excitation energies are Green’s functions methods such as many-body perturbation theory (GW)^{1,2} or wavefunction methods such as quantum Monte Carlo³ and equation-of-motion coupled cluster⁴ — although for the latter, calculations for the solid state (rather than for molecules) are far from routine. Of these approaches, GW is computationally the least expensive, scaling as $\mathcal{O}(N^4)$, where N is the number of electrons in the system.

Despite ongoing progress in the field of GW,⁵ performing these calculations is not straightforward. The aforementioned scaling of $\mathcal{O}(N^4)$ can still be an obstacle, and the calculations themselves can be challenging: they converge slowly with respect to the number of empty states included (which increases the importance of constructing transferable pseudopotentials that avoid ghost states⁶), and there is a strong interdependence of the results on different calculation parameters, which makes achieving convergence challenging at best. This hampers routine applications of GW (especially in a high-throughput context, where the calculations must be unsupervised).⁷ Finally, while in principle GW and many-body perturbation theory are systematically improvable — that is to say, by increasing the number of diagrams included in the calculations, the results should progressively converge to the correct answer (with GW outperforming GW_0 in turn outperforming G_0W_0) — in practice this does not appear to hold.⁸

Alternatively, one could try and calculate the energies of electronic excitations with density functional theory (DFT). DFT has proven to be a remarkably successful theory for predicting the properties of solids, surfaces, nanoparticles, and molecules.^{9,10} It is typically inexpensive, and these days such calculations are generally robust and can be treated as a “black box”. However, DFT is a theory of total energies, and while the Kohn-Sham auxiliary system is a powerful construct, the Kohn-Sham eigenvalues are not necessarily related to the energies of charged excitations (with the exception of the highest occupied molecular orbital, or HOMO, which is related to the exponential decay of the density¹¹). Nevertheless,

these eigenvalues can bear qualitative or even quantitative resemblance to experimental quasiparticle energies, and it is common practice to interpret them as such, motivated by the fact that the Kohn-Sham potential is the best local and static approximation to the electronic self-energy.¹² Besides from this theoretical disconnect, problems also arise from the additional approximations inherent in exchange-correlation functionals. In the case of local and semi-local functionals, a key qualitative failure arises from the erroneous convex curvature in the total energy as a function of the total number of electrons in the system, which should instead be piecewise-linear.¹³ This curvature explains in part the disagreement between first ionization potentials as calculated via total energy differences compared to Kohn-Sham eigenvalues.

Many strategies have emerged that attempt to restore the piecewise linearity of the energy functional — the hope being that the resulting Kohn-Sham eigenvalues will yield accurate excitation energies. For example, DFT+ U imposes a penalty functional to a localized subspace that restores linearity in the energy with respect to the occupation of this subspace.^{14,15} Similarly, hybrid functionals mix semi-local functionals with Hartree-Fock exchange (which happens to exhibit a concave curvature), which means that for a specific mixing fraction of the two functionals there will be an overall error cancellation.^{16–19} Recent state-of-the-art approaches that employ curvature corrections to yield reliable quasiparticle energies include screened, range-separated, and dielectric-dependent hybrid functionals with tuned mixing or range-separation parameters,^{20–25} as well as the Koopmans-Wannier method of Wang and coworkers²⁶ and the localized orbital scaling correction (LOSC) of Yang and coworkers.^{27–29} Piecewise linearity is also central to ensemble density functional theory.^{30,31} Even DM21, the recent machine-learned exchange-correlation functional created by Google DeepMind, was constructed around the idea of restoring piecewise linearity.³²

Starting in 2009, we have introduced and developed the concept of Koopmans functionals.^{33–45} By imposing a generalized piecewise linearity condition and relating quasiparticle energies to total energy differences, these functionals address the above issues, and as a conse-

quence they yield spectroscopic properties (such as molecular ionization potentials, electron affinities, and solid-state band structures) with comparable accuracy to state-of-the-art GW approaches, but at greatly reduced computational cost. Here, we introduce `koopmans`, a package that allows non-experts to perform their own Koopmans functional calculations. To guide users, this paper provides an overview of the theory behind Koopmans functionals (Section 1), demonstrates how `koopmans` can be used to perform example calculations (Section 2), and finally describes the implementation (Section 3).

1 Koopmans functionals

1.1 Fundamental concepts

For a spectral theory, the orbital energies ε_i should match the total energy differences corresponding to electron removal $E(N) - E_i(N - 1)$ and addition $E_i(N + 1) - E(N)$. This is trivially true for the exact Green’s function, whose poles correspond directly to these total energy differences, but there is no such connection in Kohn-Sham DFT. The only exception to this is the HOMO, but even there the violation of piecewise linearity in approximate DFAs leads to a mismatch between the HOMO eigenvalue with the corresponding total energy difference (i.e. the negative of the ionization potential).

Koopmans functionals restore this correspondence, by imposing the condition that the energies $\varepsilon_i = \langle \varphi_i | \hat{H} | \varphi_i \rangle = \frac{dE}{df_i}$ of orbitals φ_i should be independent of that orbital’s occupation f_i :

$$\varepsilon_i = \text{constant with respect to } f_i \tag{1}$$

It follows from Janak’s theorem that this is equivalent to a “generalized” piecewise linearity condition where the total energy of the system is piecewise linear with respect to the change of occupation of *any* orbital. This is a sufficient but not a necessary condition to fulfil the much more well-known piecewise linearity condition,⁴⁶ which states that the total energy of

the system is piecewise linear with respect to its *total* number of electrons.

Imposing this condition will require a beyond-DFT approach (and is not simply a matter of correcting density functional approximations within a DFT framework). We can see this if we consider the exact density functional, for which the negative of the HOMO energy matches the ionization potential, but there is no such guarantee for the other eigenenergies.¹¹ Consequently, imposing this condition will require corrections that are non-vanishing even for the exact density functional.

This generalized piecewise linearity condition of Equation 1 is imposed on a “base” functional (here, approximate or exact DFT) by removing, orbital-by-orbital, the non-linear dependence of the energy E on the orbital occupation f_i and replacing it with a term that is linear in f_i :

$$E^{\text{Koopmans}} = E^{\text{DFT}} + \sum_i \left[- \left(E^{\text{DFT}} - E^{\text{DFT}}|_{f_i=0} \right) + f_i \eta_i \right] \quad (2)$$

where $E^{\text{DFT}}|_{f_i=f}$ corresponds to the DFT energy of the $(N - 1 + f)$ -electron system, with the occupancy of orbital i constrained to be f . Here, the first term in the square brackets removes the dependence of the total energy on f , and the second term replaces it with a term explicitly linear in f . Here, one must choose a suitable slope η_i for this linear term; one option is to use the energy difference between fully-occupied and empty orbitals

$$\eta_i^{\text{KI}} = E^{\text{DFT}}|_{f_i=1} - E^{\text{DFT}}|_{f_i=0} \quad (3)$$

giving rise to the Koopmans integer (KI) functional. Note that this formulation provides Koopmans functionals with meaningful eigenvalues, because they now correspond to total energy differences (which in the scope of DFT are meaningful and much more reliable than Kohn-Sham eigenvalues).

Equations 2 and 3 are difficult to evaluate unless we only consider the explicit dependence of the DFT energy on the orbital occupancies, neglecting the orbital response to their

changing occupation, in which case

$$E^{\text{DFT}} - E^{\text{DFT}}|_{f_i=0} = E^{\text{DFT}}[\rho] - E^{\text{DFT}}[\rho - \rho_i] \quad (4)$$

where $\rho_i = f_i|\varphi_i|^2$ is the occupancy-weighted density of orbital i . Orbital relaxation — or, equivalently, screening — is instead accounted for *post hoc* by scaling down the unscreened correction by a scalar coefficient α_i . Crucially, these coefficients can be calculated *ab initio* at the level of DFT via linear response or total energy differences.^{41,42} This brings us, finally, to the Koopmans energy functional:

$$E^{\text{Koopmans}}[\rho, \{\rho_i\}] = E^{\text{DFT}}[\rho] + \sum_i \alpha_i [- (E^{\text{DFT}}[\rho] - E^{\text{DFT}}[\rho - \rho_i]) + f_i\eta_i] \quad (5)$$

The full derivation of Equation 5 can be found in Supporting Information S1. This functional is actually very different from semi-local DFT functionals; this will be elaborated upon in the following sections.

1.2 Orbital-density dependence

The one important distinction that is worth making right away is that Koopmans functionals are not density functionals, but *orbital-density-dependent* (ODD) functionals. This is because they are dependent on the individual orbital densities $\{\rho_i\}$. Each orbital is subject to a different potential, and when we minimize a Koopmans functional we must minimize the total energy with respect to the entire set of orbitals, as opposed to just the total density.

One characteristic of ODD functional theories (ODDFTs) is that they can give rise to *two* sets of orbitals that we must be careful to distinguish. The set of orbitals that minimize the total energy are called *variational* orbitals. These variational orbitals tend to be very localized (see Figure 1a).

Having minimized the Koopmans functional one can then construct the Hamiltonian. If we then diagonalize this Hamiltonian we would obtain the so-called *canonical* orbitals. In

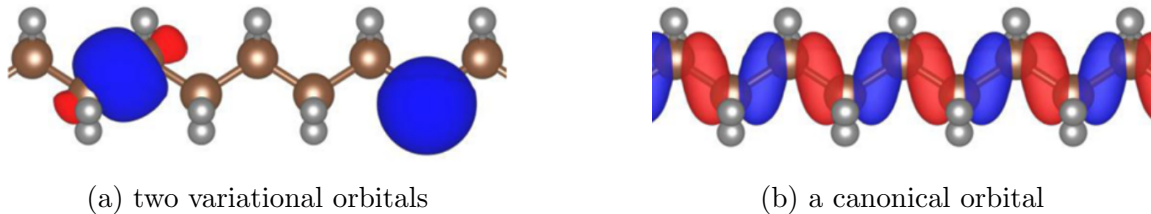


Figure 1: Variational and canonical orbitals of polyethylene. Figure taken from Ref. 41.

contrast to the variational orbitals, the canonical orbitals are not localized and much more closely resemble the Kohn-Sham orbitals of DFT (see Figure 1b). In a solid, they satisfy Bloch's theorem.⁴³ In a DFT framework, the energy of the system is the same if we evaluate it using the canonical orbitals or the variational orbitals, because the energy depends only on the total density. However, in an ODDFT, this is not the case: the total energy is not invariant with respect to unitary rotations of a given set of orbitals, and thus the ODD energy differs depending on which set of orbitals it is evaluated.

Moving from a DFT framework to an ODDFT framework, and having to now keep track of these two different sets of orbitals, may appear like a painful complication – or even an unhelpful one. This is not the case; ODDFTs come with several notable advantages. Firstly, ODDFTs are a very natural way to generalize DFT to predict spectral information. Ultimately, the spectral properties of a many-body electronic system is exactly described by its non-local and dynamic self-energy. The exact Kohn-Sham potential is the best local and approximation to this self-energy.¹² If we instead consider local but dynamic approximations, one enters into the domain of spectral functional theories, where the exact spectral functional predicts exactly the spectral density $\rho(\mathbf{r}, \omega)$.⁴⁷ ODDFTs can be interpreted as energy-discretized spectral functional theories,³⁷ so as such an ODDFT framework is a sensible choice when attempting to predict spectral properties. Secondly, it is very apt that the ODD formalism naturally gives rise to a set of localized orbitals when it comes to dealing with periodic systems. By applying Koopmans corrections to a set of localized orbitals, the corrections are well-defined and non-vanishing for both small molecules, infinite bulk sys-

tems, and everything in between. Contrast this to if we were to apply the corrections to the canonical orbitals, in which case they would become ill-defined in the bulk limit. For a more detailed discussion on this topic, see Supporting Information S2.

Nevertheless, the canonical orbitals and the corresponding eigenvalues are always interpreted as Dyson orbitals and quasiparticle energies. Note that this means that the reliability of quasiparticle energies (and their correspondence with total energy differences) is not directly imposed, but instead is inherited via the variational orbitals. That is to say: the Koopmans corrections are applied to the variational orbitals, and thus the Koopmans functional is linear with respect to the occupancy of variational orbitals. The canonical orbitals are composed of some linear combination of variational orbitals, and their energies (i.e. the quasiparticle energies) will be subject to some weighted combination of corrective potentials arising from their constituent variational orbitals.

1.3 Accounting for screening effects

As we discussed earlier in Section 1.1, we account for orbital relaxation *post hoc* via screening parameters $\{\alpha_i\}$ and we can calculate these parameters *ab initio*. But how?

The crucial point is that we would like the total energy to be piecewise linear *i.e.* we would like orbital energies (specifically, the expectation value of the Hamiltonian on a particular variational orbital) to match the corresponding total energy differences when adding/removing an electron from this orbital, without the frozen-orbital assumption that we made earlier. Specifically, we would like $\lambda_{ii}(\alpha, f) = \Delta E_i^{\text{Koopmans}}$, where

$$\lambda_{ii}(\alpha, f) = \langle \varphi_i | \hat{h}^{\text{DFT}} + \alpha \hat{v}^{\text{Koopmans}} | \varphi_i \rangle \Big|_{f_i=f} = \frac{\partial E^{\text{Koopmans}}}{\partial f_i} \Big|_{f_i=f} \quad (6)$$

is the expectation value of the Hamiltonian for a given variational orbital φ_i , and

$$\Delta E_i^{\text{Koopmans}} = \begin{cases} E^{\text{Koopmans}}(N) - E_i^{\text{Koopmans}}(N-1) & \text{for occupied orbitals} \\ E_i^{\text{Koopmans}}(N+1) - E^{\text{Koopmans}}(N) & \text{for empty orbitals} \end{cases} \quad (7)$$

where $E_i^{\text{Koopmans}}(N \pm 1)$ is the total energy of the system where we add/remove an electron from variational orbital i and allow the rest of the system to relax, with all the other orbitals remaining orthogonal to $|\varphi_i\rangle$.

We will use this condition to determine the screening parameters *ab initio*. In order to do so, there are two potential approaches: (a) via finite difference calculations or (b) via density functional perturbation theory (DFPT).

1.3.1 Screening from finite-differences

In this approach, we explicitly calculate all of the energy differences $\Delta E_i^{\text{Koopmans}}$ via a series of constrained Koopmans or DFT calculations. Specifically, given a starting guess $\{\alpha_i^0\}$ for the screening parameters, an improved guess for the screening parameters can be obtained via

$$\alpha_i^{n+1} = \alpha_i^n \frac{\Delta E_i - \lambda_{ii}(0, 1)}{\lambda_{ii}(\alpha_i^n, 1) - \lambda_{ii}(0, 1)}; \quad \Delta E_i = E(N) - E_i(N-1) \quad (8)$$

for occupied orbitals and

$$\alpha_i^{n+1} = \alpha_i^n \frac{\Delta E_i - \lambda_{ii}(0, 0)}{\lambda_{ii}(\alpha_i^n, 0) - \lambda_{ii}(0, 0)}; \quad \Delta E_i = E_i(N+1) - E(N) \quad (9)$$

for empty orbitals, where $E_i(N \pm 1)$ is the total energy of the $N \pm 1$ electron system where we take the N -electron system, take this variational orbital i and fill/empty it, and then hold it frozen while the rest of the system is allowed to relax (while remaining orthogonal). These equations yield the screening parameters that satisfy $\lambda_{ii}(\alpha, f) = \Delta E_i^{\text{Koopmans}}$ if we assume a linear dependence of λ_{ii} on α_i and approximate the total energy as a function of f_i

to second order. By iterating to self-consistency we lift these approximations and guarantee that $\lambda_{ii}(\alpha, f) = \Delta E_i^{\text{Koopmans}}$ is satisfied. Typically, only a few iterations are required in order to reach self-consistency, especially if one starts from a physically-motivated initial guess (such as the static limit of the inverse dielectric function ϵ^{-1} in the case of bulk systems).

All of these ingredients for calculating α_i^{n+1} are obtained from constrained Koopmans and DFT calculations. Specifically, a N -electron Koopmans calculation yields $E^{\text{Koopmans}}(N)$ and $\lambda_{ii}(\alpha, f)$ (for both $\alpha = \alpha_i^n$ and 0, and $f = 1$ for filled orbitals and 0 for empty). Meanwhile, a constrained $N \pm 1$ -electron calculation yields $E_i^{\text{Koopmans}}(N \pm 1)$.

For a periodic system, this method for determining the screening parameters requires a supercell treatment. This is because the $N \pm 1$ -electron systems contain a charged defect (because we have filled/emptied a localized orbital) and a supercell is required in order to remove the spurious interactions between periodic images.^{41,43}

1.3.2 Screening from density-functional perturbation theory

While the finite-difference approach can provide us with all of the ingredients to calculate the screening parameters, it is somewhat cumbersome, since one must perform several constrained DFT and Koopmans calculations, and for periodic systems these must be performed in a supercell. An alternative to this approach is to compute the screening coefficients via density-functional perturbation theory (DFPT).⁴⁸

In this approach, one first approximates the energy as a quadratic function of the occupation number, and the expression for the screening coefficients reduces to

$$\alpha_i = \frac{d^2 E_{\text{DFT}}/df_i^2}{\partial^2 E_{\text{DFT}}/\partial f_i^2} = \frac{\langle n_i | \epsilon^{-1} f_{\text{Hxc}} | n_i \rangle}{\langle n_i | f_{\text{Hxc}} | n_i \rangle}, \quad (10)$$

where $\frac{d}{df_i}$ and $\frac{\partial}{\partial f_i}$ represent variations done accounting for the orbitals relaxation or not, respectively, $\epsilon(\mathbf{r}, \mathbf{r}')$ is the microscopic dielectric function of the material, $f_{\text{Hxc}}(\mathbf{r}, \mathbf{r}') = \delta^2 E_{\text{Hxc}}/\delta\rho(\mathbf{r})\delta\rho(\mathbf{r}')$ is the Hartree-plus-exchange and correlation kernel, and $n_i(\mathbf{r}) = |\varphi_i(\mathbf{r})|^2$

is the orbital density.⁴² This can be evaluated by considering the density response $\Delta^i n(\mathbf{r})$ induced in the system by the perturbing potential $v_{\text{pert}}^i(\mathbf{r}) = \int d\mathbf{r}' f_{\text{Hxc}}(\mathbf{r}, \mathbf{r}') n_i(\mathbf{r}')$. This perturbation is the Hartree-plus-exchange-correlation potential generated when adding/removing an infinitesimal fraction of an electron to/from orbital i . One determines $\Delta^i n$ self-consistently via DFPT,⁴⁹ and then the screening parameters are given by

$$\alpha_i = 1 + \frac{\langle v_{\text{pert}}^i | \Delta^i n \rangle}{\langle n_i | v_{\text{pert}}^i \rangle}. \quad (11)$$

Evaluating the screening coefficients within this linear-response approach only requires quantities available from a N -electron calculation, which means that in the case of periodic solids there is no need for a supercell. Instead, we can exploit the translational symmetries of the system, recast the problem within the primitive cell, and thereby dramatically reduce its computational cost. This will be discussed later in Section 3.2.2. However, the DFPT approach does come with some limitations. The principal limitation is that the energy is approximated to second order in the perturbing potential. In most cases this is very accurate, correctly capturing the leading Hartree contribution and only missing higher-order exchange-correlation contributions.

1.4 Flavors

As we saw previously in Section 1.1, there is some freedom in how one defines a Koopmans functional. Namely, one must choose values for η_i , the gradient of the energy as a function of the the occupancy of orbital i , for each value of i (modulo the corresponding screening term). In that section, we briefly introduced the Koopmans integer (KI) approach (Equation 3), but that is just one of several different ways one can define these gradient terms, and each approach gives rise to a different “flavor” of Koopmans functionals.

1.4.1 KI

In the KI approach, η_i is chosen as the total energy difference of two adjacent electronic configurations with integer occupations as given by the base DFT functional:

$$\eta_i^{\text{KI}} = E^{\text{DFT}}|_{f_i=1} - E^{\text{DFT}}|_{f_i=0} = \int_0^1 \langle \varphi_i | \hat{h}^{\text{DFT}}(f) | \varphi_i \rangle df \quad (12)$$

where $\hat{h}^{\text{DFT}}(f)$ is the DFT Hamiltonian with the occupancy of orbital i constrained to f . In this case, the explicit expression for the unscreened KI Koopmans' correction to orbital i , which we denote as Π_i^{KI} , becomes

$$\Pi_i^{\text{KI}} = E_{\text{Hxc}}[\rho - \rho_i] - E_{\text{Hxc}}[\rho] + f_i (E_{\text{Hxc}}[\rho - \rho_i + n_i] - E_{\text{Hxc}}[\rho - \rho_i]) \quad (13)$$

where $\rho_i(\mathbf{r}) = f_i |\varphi_i(\mathbf{r})|^2$ and $n_i(\mathbf{r}) = |\varphi_i(\mathbf{r})|^2$. E_{Hxc} denotes the Hartree and exchange-correlation energy corresponding to the underlying base functional.

It can be seen that at integer occupations, the KI energy correction vanishes i.e. $\Pi_i^{\text{KI}} = 0$. In other words, for integer occupations the KI functional preserves the potential energy surface of the base functional! But while the energy correction is vanishing, the potential is non-vanishing, which means that the KI correction will affect the spectral properties of the system.

1.4.2 KIPZ

In the ‘‘KIPZ’’ approach, the slope η_i is also chosen as the total energy difference of two adjacent electronic configurations with integer occupations, but this time using the Perdew-Zunger (PZ) one-electron-self-interaction corrected (SIC) functional applied to the approximate DFT base functional:

$$\eta_i^{\text{KIPZ}} = E^{\text{PZ}}|_{f_i=1} - E^{\text{PZ}}|_{f_i=0} = \int_0^1 \langle \varphi_i | \hat{h}_i^{\text{PZ}}(s) | \varphi_i \rangle ds, \quad (14)$$

In this instance, the explicit expression for the unscreened energy correction corresponding to orbital i (denoted Π_i^{KIPZ}) becomes

$$\Pi_i^{\text{KIPZ}} = - \int_0^{f_i} \langle \varphi_i | \hat{h}^{\text{DFT}}(f) | \varphi_i \rangle df + f_i \int_0^1 \langle \varphi_i | \hat{h}_i^{\text{PZ}}(f) | \varphi_i \rangle df, \quad (15)$$

where

$$\hat{h}_i^{\text{PZ}}(f) = \hat{h}^{\text{DFT}}(f) - \hat{v}_{\text{Hxc}}^{\text{DFT}} [f |\varphi_i(\mathbf{r})|^2] \quad (16)$$

is the PZ self-interaction correction applied to the i^{th} variational orbital with constrained occupation f , which removes the Hartree-plus-exchange-correlation potential for that orbital. The KIPZ correction can be rewritten as

$$\Pi_i^{\text{KIPZ}} = \Pi_i^{\text{KI}} - f_i E_{\text{Hxc}}[n_i] \quad (17)$$

which makes the physics of this correction clear: it is nothing less than the KI correction with the addition of a (screened) Perdew-Zunger self-interaction correction. This added correction removes one-electron self-interaction and makes the KIPZ functional exact for one-electron systems.

1.4.3 KI versus KIPZ, and pKIPZ

The KIPZ correction is more computationally expensive than the KI approach, for the following reasons: we have already mentioned that the KI energy correction vanishes for integer orbital occupations. Furthermore, for occupied orbitals, the KI corrective potential is scalar (i.e. it does not have a spatial dependence) and therefore the total energy is invariant with respect to unitary rotations of the variational orbitals. Consequently, once the variational orbitals (and, by extension, the total density) are initialized they remain unchanged during the entire energy minimization procedure. This also implies that the screening parameters of occupied variational orbitals converge instantly. (In equation 8, ΔE_i and $\lambda_{ii}(0,1)$ are

independent of α_i^n and $\lambda_{ii}(\alpha_i^n, 1)$ is linear in α_i^n .) Contrast this with KIPZ: the KIPZ energy does not match that of the base functional, nor is it invariant with respect to the unitary rotations of occupied orbitals. This means we must directly minimize the energy with respect to the shape of the variational orbitals. Furthermore, the KIPZ ground-state density and variational orbitals are a function of the screening parameters.

Despite its additional computational cost, KIPZ has some desirable advantages over KI: for instance, it is one-electron-self-interaction-free. For this reason, we also have introduced the “perturbative KIPZ” (pKIPZ) method, where the KIPZ Hamiltonian is applied non-self-consistently to the KI density and variational orbitals, as a way of approximating the KIPZ result at reduced computational cost without significantly compromising the accuracy.⁴⁴

Finally, we note that the KI functional’s invariance with respect to unitary rotations of the variational orbitals introduces an ambiguity in its definition: the variational orbitals are no longer well-defined. This ambiguity is resolved by formally defining the KI functional as the $\gamma \rightarrow 0$ limit of the “KI γ PZ” functional, which is the KIPZ functional with the PZ contribution to the correction scaled by a prefactor γ . This is discussed further in the Supporting Information S3.1.1.

1.4.4 Other flavors

The original formulations of Koopmans functionals also introduced the K and the KPZ functionals.^{33,34,36} These are similar to the KI and KIPZ functionals, except that the slope η_i is evaluated at half-occupation rather than as the total energy difference between integer occupations. These formulations are more cumbersome than their integer counterparts, and are no longer used.

1.5 Other considerations

Before concluding this section, there are a few further important points that must be made.

1.5.1 Restriction to systems with a non-zero band gap

Firstly, the Koopmans formulation is only well-defined for systems that have a non-zero band gap. This is because the Koopmans correction (Equation 6) is defined in terms of the diagonal elements of the occupation matrix. A band gap (however small) means that the occupancy matrix is block-diagonal, and can always be chosen to be the identity for the occupied manifold and zero for the unoccupied manifold. In the absence of a band gap, the occupancy matrix is not block-diagonal and a well-defined Koopmans functional would require some (currently unknown) corrections for the off-diagonal components.

While it would be desirable to derive an off-diagonal correction and to lift this restriction, the current theory remains powerful — after all, it is in insulating and semi-conducting systems where DFT exhibits one of its most striking failures in the underestimation of the band gap.

1.5.2 Empty state localization in the bulk limit

While minimizing the Koopmans energy functional for bulk systems leads to well-localized occupied orbitals, the same process does not lead to well-localized empty orbitals. This is because (a) low-lying conduction bands are often entangled with highly-delocalized nearly-free-electron bands, and (b) the Koopmans correction to empty states contains a leading Hartree term that incentivizes delocalization (see Ref. 36). However, the Koopmans correction ought to be applied to localized orbitals, and vanishes in the limit of infinitely delocalized states (see Supporting Information S2). In light of this, we typically apply the Koopmans correction non-self-consistently on a maximally localized Wannier function representation of the empty manifold. This approach is heuristic but effective, as demonstrated by previous works.^{41,43}

1.6 Workflows

In a (semi-)local DFT calculation, all that one needs to do is determine the ground-state density. For Koopmans calculations one must also obtain the minimizing variational orbitals as well as the screening parameters. This means that, compared to a standard semi-local DFT calculation, a few additional steps are required. Typically, a Koopmans calculation can be divided into three steps:

1. an initialization step, where the density and variational orbitals are initialized
2. the calculation of screening parameters
3. a final calculation using the final screening parameters

Depending on the method used for calculating screening parameters (that is, either finite differences or DFPT), the resulting workflow looks very different. Differences also emerge between calculations on molecules and solids. For the latter (and for large molecular systems), maximally localized Wannier functions are typically used as the variational orbitals (for KI) or as a starting guess for the variational orbitals (for KIPZ). This necessitates an additional Wannierization procedure.⁵⁰ In all cases, the workflows typically comprise of several if not dozens of calculations, often involving different electronic structure codes that must handshake with one another. For a comprehensive explanation of the Koopmans workflows, refer to Supporting Information S3.

2 Example calculations

This Koopmans functional formalism has already proven to be very powerful. In Ref. 44, Koopmans functionals were found to predict the ionization potentials of a set of 100 small molecules with comparable/superior accuracy to state-of-the-art GW approaches. Importantly, Koopmans functionals do not only correct the ionization potential (i.e. the charged

excitation where the most weakly bound electron is removed) but *any* single-particle charged excitation. This was shown for a large set of molecules relevant for photovoltaic applications,³⁹ with Koopmans functionals yielding ultraviolet photoemission spectra that agree quantitatively with experiment. One can see similar accuracy in the prediction of band gaps and band structures of periodic systems;^{41,43,49} in a study of prototypical semiconductors and insulators, Koopmans functionals were found to yield band gaps with a mean absolute error of 0.22 eV, compared to 0.18 eV when using self-consistent GW with vertex corrections.⁴¹ Importantly, alignment between the valence band edge and the vacuum level was also very good: across six semiconductors the mean absolute error was 0.19 eV, compared to 0.39 eV for G_0W_0 and 0.49 eV for self-consistent GW with vertex corrections.

The Koopmans formalism that underpins all of these calculations is inherently more complex than a semi-local DFT algorithm (e.g. it asks for the optimization of variational orbitals in addition to the total density), requiring custom implementation within electronic structure codes. These calculations also required complicated workflows (e.g. for calculating screening parameters), and as such, they can greatly benefit from automation. This has been implemented as the `koopmans` package. In the next section, we will discuss how this was implemented, but first, this section introduces the capabilities of the `koopmans` package by way of several examples.

Note that the following calculations use slightly underconverged parameters (specifically, the energy cutoff, cell size, and/or the size of the k -point grid). Our focus here is to provide example calculations that can be reproduced easily by readers, rather than providing high-quality reference results.

2.1 The ionization potential and electron affinity of ozone

In this section, we give a brief overview of how to calculate the ionization potential and electron affinity of ozone using `koopmans`.

2.1.1 The input file

koopmans takes a single input file in JSON format. An example minimal input file for ozone is as follows

```
1 {
2   "workflow": {
3     "functional": "ki",
4     "method": "dscf",
5     "init_orbitals": "kohn-sham",
6     "n_max_sc_steps": 5,
7     "keep_tmpdirs": false,
8     "pseudo_library": "sg15"
9   },
10  "atoms": {
11    "cell_parameters": {
12      "periodic": false,
13      "vectors": [[14.1738, 0.0, 0.0],
14                  [0.0, 12.0, 0.0],
15                  [0.0, 0.0, 12.66]],
16      "units": "angstrom"
17    },
18    "atomic_positions": {
19      "positions": [{"O", 7.0869, 6.0, 5.89],
20                   ["O", 8.1738, 6.0, 6.55],
21                   ["O", 6.0, 6.0, 6.55]},
22      "units": "angstrom"
23    }
24  },
25  "calculator_parameters": {
26    "ecutwfc": 65.0,
27    "nbnd": 10
28  }
29 }
```

This input file contains several blocks. The `workflow` block allows the user to specify the details of the workflow. Here we can see we are performing a KI calculation (line 3) calculating the screening parameters via the finite-difference procedure (line 4), and using the Kohn-Sham orbitals to initialize our variational orbitals (line 5; this is common practice for molecules). The `atoms` block (lines 10-23) contains standard keywords specifying the

system configuration, such as the `cell_parameters` and `atomic_positions`. These mirror the equivalent blocks in Quantum ESPRESSO input files (albeit in JSON format). Finally, the `calculator_parameters` block allows the user to specify settings specific to a particular code (e.g. a `w90` subblock for specifying Wannier90 settings). In this instance we are providing a particular energy cutoff (line 26) and specifying the total number of orbitals to compute (line 27).

2.1.2 Running the calculation

This calculation is run with the simple command `koopmans ozone.json`, the output of which can be seen in Supporting Information S4.1. In short, the command prompts the full sequence of Quantum ESPRESSO calculations necessary to initialize the density and variational orbitals, calculate the screening parameters, and run a final KI calculation. The Quantum ESPRESSO input and output files for these calculations are all stored in various subdirectories of the current working directory. In principle one can then simply parse the quantities of interest from the output files (but there are easier ways, as we will see in Section 3.1.2).

The ionization potential (IP) and electron affinity (EA) of ozone, as given by the above calculation, are listed in Table 1, showing the excellent performance of the KI functional compared to state-of-the-art methods.

2.2 The band structure of silicon

`koopmans` can also perform calculations on bulk systems. As mentioned in Section 1.6, here one typically performs a Wannierization procedure in order to generate maximally localized Wannier functions to use as variational orbitals. A typical input file for silicon similar to that of ozone but with some tweaked workflow settings, a `cell_parameters` block that denotes that this system is periodic, and some additional Wannierization settings:

```
33     "w90": {
34         "projections": [
35             [{"fsite": [0.25, 0.25, 0.25], "ang_mtm": "sp3"}],
```

Table 1: The vertical ionization potential (IP) and electron affinity (EA) of ozone, as calculated using functional, perturbative, and quantum chemistry methods, as well as experiment. KI@[PBE,KS] denotes the KI Koopmans correction on top of the PBE base functional, with Kohn-Sham orbitals defining the variational orbitals, showing excellent performance compared to state-of-the-art methods. The uncertainties in the G_0W_0 correspond to the standard deviation of values reported in Ref. 51, which presents calculations using a range of codes and basis sets.

	IP	EA	
PBE	7.95	6.17	This work
G_0W_0	11.80 ± 0.25	2.34 ± 0.25	Ref. 51
scGW ₀ @PBE	12.57		Ref. 52
scGW ₀ @HF	13.16		Ref. 52
scGW	12.54		Ref. 52
qsGW	13.21		Ref. 52
CCSD(T)	12.55		Ref. 53
KI@[PBE,KS]	12.52	1.82	This work
KI@[PBE,KS]	12.91		Ref. 44
experiment	12.73	2.10	Refs. 54–57

```

36     [{"fsite": [0.25, 0.25, 0.25], "ang_mtm": "sp3"}],
37     "dis_froz_max": 11.0,
38     "dis_win_max": 16.5
39   },
40   "ui": {
41     "smooth_int_factor": 2
42   }

```

(See the Supporting Information for the full input file; for a full explanation of the meaning of these Wannier90 keywords we refer the reader to the Wannier90 documentation). Running this calculation gives rise to a similar output to the previous case, with the notable exception that the initialization procedure now involves Wannierization (see Supporting Information S4.2). The band structure that one obtains from this calculation is shown in Figure 2 and the band gap is displayed in Table 2 alongside those obtained via other methods.

2.3 The band structure of zinc oxide

The previous example used the finite-difference approach for calculating the screening parameters. In this final example of zinc oxide, we will instead use the DFPT approach. The

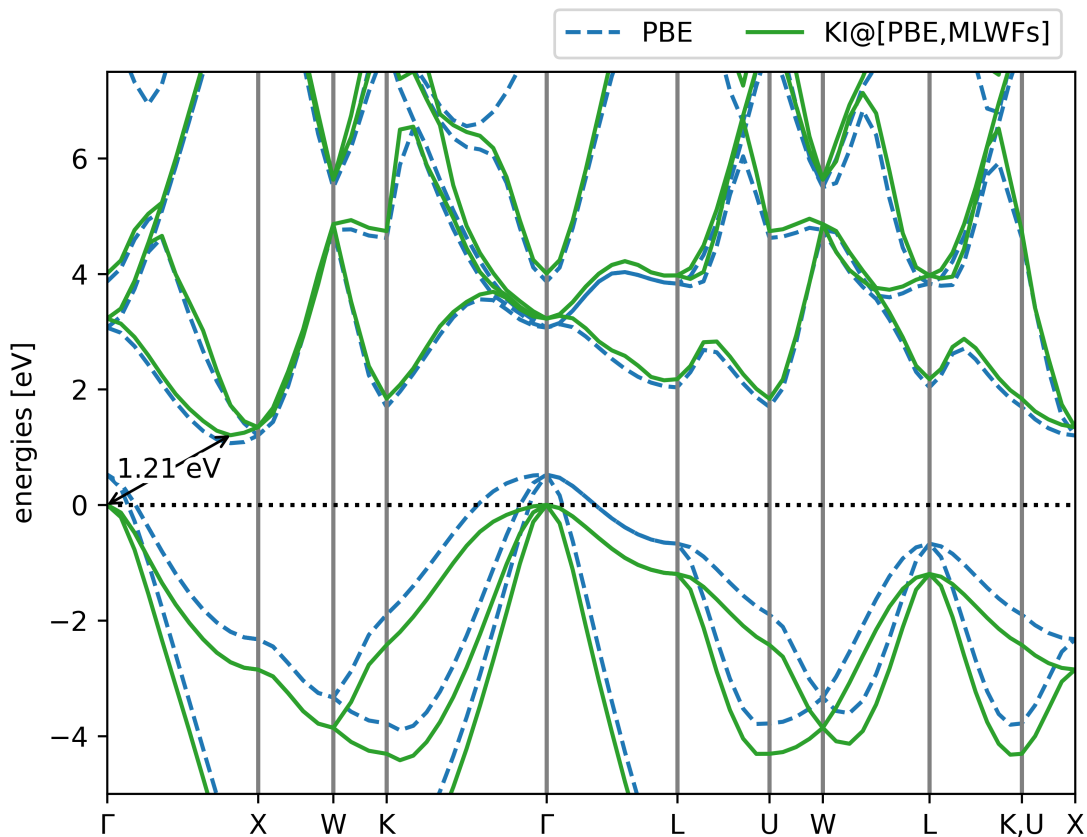


Figure 2: Band structure of bulk silicon, calculated using the KI functional with the PBE base functional, MLWFs as variational orbitals, and screening parameters calculated via finite differences. The PBE band structure is also plotted for comparison.

workflow block of the input file is as follows:

```

1 {
2   "workflow": {
3     "task": "singlepoint",
4     "functional": "ki",
5     "base_functional": "lda",
6     "method": "dfpt",
7     "init_orbitals": "mlwfs",
8     "calculate_alpha" : true,
9     "pseudo_library": "pseudo_dojo_standard",
10    "gb_correction" : true,
11    "eps_inf": 5.3,
12    "from_scratch": true,
13    "npool": 4,
14    "dfpt_coarse_grid": [2, 2, 2],

```

Table 2: The band gap (eV) of bulk silicon, as given by various functional and perturbative approaches, as well as experiment. The experimental value listed has been shifted by -0.05 eV to account for zero-point renormalisation.⁶¹

PBE	0.68	This work
G_0W_0	1.12	Ref. 58
GW_0	1.20	Ref. 58
sc $G\tilde{W}$	1.24	Ref. 59
KI@[PBE,MLWFs]	1.18	Ref. 43
KI@[PBE,MLWFs]	1.21	This work
experiment	1.23	Ref. 60

Table 3: The band gap (eV) of bulk zinc oxide, as given by various functional and perturbative approaches, and compared to experiment. The experimental value listed has been shifted by -0.16 eV to account for zero-point renormalisation.⁶³ Importantly, the result of Ref. 49 used finer parameters than this work (most notably, a $6 \times 6 \times 6$ k -point grid throughout).

LDA	0.69	This work
G_0W_0	3.0	Ref. 58
GW_0	3.0	Ref. 58
sc $G\tilde{W}$	3.2	Ref. 59
KI@[LDA,MLWFs]	3.62	Ref. 49
KI@[LDA,MLWFs]	3.51	This work
experiment	3.60	Ref. 62

```

15     "orbital_groups_spread_tol": 0.0005
16 }

```

Here we can see the selection of DFPT for calculating screening parameters (line 6), the choice of MLWFs as the variational orbitals (line 7), and a criterium for grouping variational orbitals together based on their spreads (line 15). We also have specified a coarse $2 \times 2 \times 2$ k -point grid on which to calculate the screening parameters (line 14) relative to the $4 \times 4 \times 4$ grid upon which we construct the Hamiltonian (specified elsewhere in the output file). Again, it is worth stressing that these calculations are underconverged.

The resulting band structure is shown in Figure 3 and the band gaps are listed in Table 3.

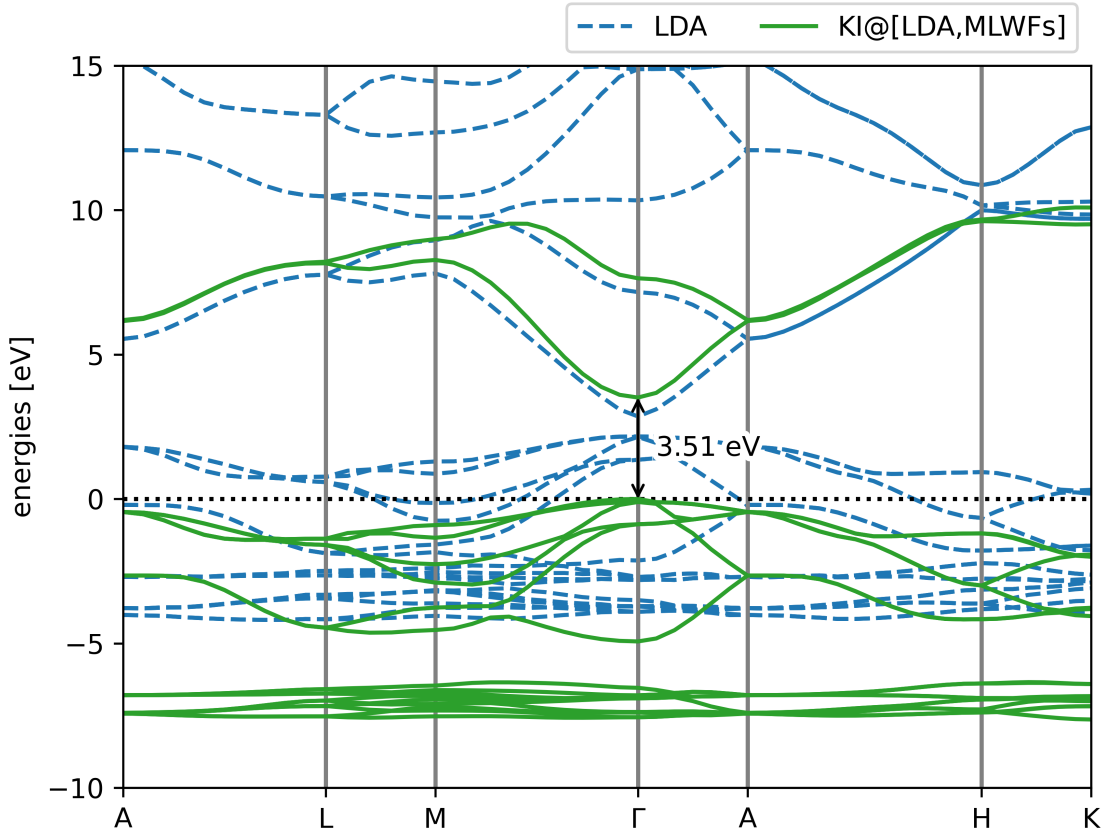


Figure 3: Band structure of zinc oxide, calculated using the KI functional with the LDA base functional, MLWFs as variational orbitals, and screening parameters calculated via DFPT. The LDA band structure is also plotted for comparison.

3 Implementation

Having introduced the core capabilities of `koopmans`, this section will now discuss the contents of the `koopmans` package in detail.

The `koopmans` package comprises three distinct sets of codes. These are a python package that automates Koopmans workflows, and two independent implementations of Koopmans functionals in `QUANTUM ESPRESSO`.^{64,65}

3.1 The workflow runner

The `koopmans` python package is responsible for running the various workflows. It is built on top of the `ASE` python package (the Atomic Simulation Environment).⁶⁶ Users exclusively interact with this workflow runner, rather than the `Quantum ESPRESSO` implementations directly. The command `koopmans <seed>.json` is a call to the workflow runner.

Based on the settings provided in the input JSON file, the workflow runner proceeds through the requested workflow. Whenever an electronic structure calculation needs to be performed, it generates a `Quantum ESPRESSO` input file, calls `Quantum ESPRESSO`, waits for it to complete, and then parses the output file. Between successive calculations, it computes intermediate variables, moves and modifies files, *etc.*. In other words, the workflow runner takes care of the banal aspects of performing a Koopmans calculation, allowing users to concern themselves with scientific matters (e.g. “what functional do I want to use?”) rather than getting bogged down in practical details (e.g. “are the Wannier function files in the correct format for the next calculation to be able to read?”)

3.1.1 Code structure

Under the hood, the workflow manager defines various `Workflow` classes, which look like

```
class Workflow:
    parameters: Dict[str, Any]
    calculations: List[Calculator]
    ...
```

where the `parameters` attribute is a dictionary that stores the workflow parameters as specified in the input file, and `calculations` is a list of the calculations in the workflow.

The individual entries in the `calculations` list correspond to `Calculator` objects:

```
class Calculator(ASE_Calculator):
    atoms: Atoms
    parameters: Dict[str, Any]
    results: Dict[str, Any]
    ...
```

which are subclasses of corresponding classes defined by ASE. ASE provides the calculator with the functionality to read and write input and output files (among many other things).

A `Calculator` object has — among others — an `atoms` attribute that stores the details of the atoms and the simulation cell. The `atoms` attribute is itself an instance of the `Atoms` class from ASE. We note that this hierarchy (namely, that the `atoms` object is an attribute of a `Calculator`, and not the other way around) is the reverse of the philosophy of ASE, where `Atoms` objects are the principal object, and they may or may not have an associated `calc` attribute.

In addition to an `atoms` attribute, `Calculator` objects also have a `parameters` attribute where calculator-specific settings are stored, as well as a `results` attribute, where the results of the calculation are stored — just like in ASE.

3.1.2 Scriptability

Because `koopmans` is written in python, integrating it within a script is straightforward. For

example, here is a script that runs the ozone calculation from Section 2.1:

```
1 from ase import build
2 from koopmans.workflows import SinglepointWorkflow
3
4 # Create an Atoms object
5 atoms = build.molecule('O3', vacuum=5.0)
6
7 # Create a koopmans Workflow object
8 workflow = SinglepointWorkflow(atoms=atoms, ecutwfc = 65.0, nbnd = 10)
9
10 # Run the workflow
11 workflow.run()
12
13 # Fetch the IP and EA
14 results = workflow.calculations[-1].results
15 ip = -results['homo_energy']
16 ea = -results['lumo_energy']
17
18 # Print the IP and EA to screen
19 print(f' IP = {ip:.2f} eV')
20 print(f' EA = {ea:.2f} eV')
```

Of course, printing the IP and EA to screen is of limited value — in reality at this stage the

user would then generate plots, or feed these results to another code.

Often a user will want to run workflows and analyse data separately — for example, they might run their workflow on remote high performance computing resources, and then, days later, analyse the results on their laptop. To permit this, `koopmans` generates a `.kwf` file when a workflow is run. This file can be loaded into python in order to recover the `Workflow` python object. For example, we could perform exactly the same analysis on our previous

ozone calculation by replacing lines 1-11 with

```
from koopmans import io
```

```
workflow = io.read('ozone.kwf')
```

where `ozone.kwf` has been generated by some previously completed `koopmans` calculation.

In the above, we used the `SinglepointWorkflow` for running a `Koopmans` workflow from start to finish. `koopmans` implements several other workflows that automate tasks that are useful when performing `Koopmans` calculations, such as convergence testing, standalone Wannierization, and DFT calculations.

3.1.3 Code quality and testing

`koopmans` contains an extensive test suite implemented with `pytest`.⁶⁷ It also has typing annotations which allow it to be statically typechecked using `mypy`.

3.2 Implementation of Koopmans functionals within Quantum ESPRESSO

Some sections of the workflows — for example, the initialization of the density, and performing Wannierization — are performed using pre-existing codes such as `pw.x`, `pw2wannier90.x`, and `wannier90.x`.^{64,65,68} However, large parts of the `Koopmans` workflows require custom code. There are two implementations of `Koopmans` functionals that the workflow runner can call upon.

3.2.1 Finite differences with orbital optimization

The first implementation of Koopmans functionals, `kcp.x`, is designed for calculating screening parameters via the finite-difference approach with full orbital optimization.

The orbital optimization is performed as follows: the orbital densities are parameterized via a set of wavefunctions ϕ_i and a unitary rotation matrix U , such that $\rho_i = |(U\phi)_i|^2$. The energy is then minimized via the nested loop:

$$E = \min_{\{\phi_i\}} \left(\min_U E^{\text{Koopmans}}[\{|(U\phi)_i|^2\}] \right) \quad (18)$$

where in the inner loop the unitary rotation matrix is optimized (which leaves the total density unchanged), and in the outer loop the wave functions are optimized. This strategy is similar to that employed in the ensemble DFT approach.⁶⁹ The minimization is performed using the conjugate gradient algorithm; further details are presented in Ref. 38.

One important ingredient in ODD energy minimization is the use of complex orbitals. Because the ODD energy is not invariant with respect to unitary rotations of the variational orbitals, it can no longer be assumed (as in the case for DFT) that the variational orbitals are real, and thus the aforementioned wave functions ϕ_i must be complex in order to find the true minimum of the ODD functional.^{36,70–73}

The finite difference procedure for calculating screening parameters requires constrained minimization calculations, where the total ODD energy is minimized while removing/adding one electron to a particular variational orbital. (This gives us $E_i(N \pm 1)$ from Equation 7). This orbital must be frozen during the minimization, otherwise it would morph into the valence band maximum/conduction band minimum, and one must also impose the standard orthogonality condition with all other orbitals belonging to the same spin channel.

For bulk systems, these $N \pm 1$ -electron constrained minimization calculations must be performed in a supercell which — in combination with an image correction method such as Martina-Tuckerman or Gygi-Baldereschi^{74,75} — avoids spurious interaction between periodic

images. The image correction methods currently implemented in `kcp.x` assume an isotropic dielectric ϵ . In the near future these will be extended to support a fully tensorial ϵ , which is critical for — among other things — calculations on two-dimensional materials. For these calculations on bulk systems (and for large molecules), Wannier functions⁵⁰ serve as a good initial guess for the variational orbitals. To support this, we have implemented an interface that takes set of \mathbf{k} -indexed Wannier functions from a `Wannier90` calculation and maps it to an enlarged set of Γ -only Wannier functions defined on the corresponding supercell.

Wherever a calculation must be performed on a supercell, \mathbf{k} -point sampling of the Brillouin zone becomes superfluous, and for this reason `kcp.x` does not implement it. Instead, the dimensions of the supercell can be used to effectively sample \mathbf{k} -space for bulk systems, and the band structure for the equivalent primitive cell can be reconstructed at the end of the calculation using an unfolding procedure.⁴³ Despite the absence of \mathbf{k} -space sampling (which is embarrassingly parallel), the `kcp.x` code still uses MPI parallelism: it is parallelized over the plane wave basis. This allows for the distribution of linear algebra operations and Fourier transforms across processors.

Given that `kcp.x` implements the full minimization of the ODD functional, in principle one could use the output of `kcp.x` to perform geometry optimizations, calculate phonons via the frozen-phonon method, calculate electron-phonon coupling, model excitons, and so on.

For historical reasons, this functionality is implemented on top of `cp.x`, the code within `Quantum ESPRESSO` usually responsible for performing Car-Parrinello molecular dynamics (hence the name “`kcp.x`”), which already contained algorithms similar to the direct functional minimization required by Koopmans functionals. It is important to note that `kcp.x` does *not* perform molecular dynamics. The implementation is built on top of version 4.1 of `Quantum ESPRESSO`. The modifications made to implement Koopmans functionals are (a) extensive and (b) of no relevance to the standard functioning of the `cp.x` code, so these modifications have not yet been incorporated within the official `Quantum ESPRESSO` repository,

nor was the private version of the code kept aligned with subsequent `Quantum ESPRESSO` releases. Fast-forward to today, and `kcp.x` has effectively become a standalone code.

3.2.2 DFPT in the primitive cell

The second implementation of Koopmans functionals in the `koopmans` package is called `kcw.x`. This code implements the calculation of screening parameters via DFPT (as presented in Section 1.3.2) and the subsequent construction of the Koopmans Hamiltonian and band structure.

`kcw.x` performs these calculations in a basis of Wannier functions (the “w” in `kcw` stands for “Wannier”). It obtains these Wannier functions via an interface with `Wannier90`. For periodic systems, these Wannier functions take the form $w^{\mathbf{R}i}(\mathbf{r})$, where the orbital label now explicitly denotes the lattice vector \mathbf{R} of the home cell inside the supercell. This choice of basis allows us to take advantage of the translational symmetry⁴³ of periodic systems: the DFPT expression for the screening coefficients (Equation 10) can be decomposed into a set of independent problems (monochromatic perturbations), one for each \mathbf{q} point sampling the Brillouin zone of the primitive cell.⁴⁹ The now \mathbf{q} -dependent charge density variation $\Delta n_{\mathbf{q}}^{\mathbf{0}i}(\mathbf{r})$ induced by the perturbing potential $v_{\text{pert},\mathbf{q}}^{\mathbf{0}i}$ is obtained self-consistently via DFPT (Equations 15-17 of Ref. 49), and then the screening coefficients are obtained by summing over \mathbf{q} :

$$\alpha_{\mathbf{0}i} = 1 + \frac{\sum_{\mathbf{q}} \langle v_{\text{pert},\mathbf{q}}^{\mathbf{0}i} | \Delta n_{\mathbf{q}}^{\mathbf{0}i} \rangle}{\sum_{\mathbf{q}} \langle n_{\mathbf{q}}^{\mathbf{0}i} | v_{\text{pert},\mathbf{q}}^{\mathbf{0}i} \rangle}. \quad (19)$$

The KI Hamiltonian at a particular \mathbf{k} point is then given to second order by

$$H_{ij}^{\text{KI}(2)}(\mathbf{k}) = H_{ij}^{\text{DFT}}(\mathbf{k}) + \alpha_{\mathbf{0}j} \Delta H_{ij}^{\text{KI}(2)}(\mathbf{k}) \quad (20)$$

where the second-order KI contribution to the Hamiltonian is

$$\Delta H_{vv'}^{\text{KI}(2)}(\mathbf{k}) = -\frac{1}{2} \langle n_{\mathbf{q}}^{\mathbf{0}v} | v_{\text{pert},\mathbf{q}}^{\mathbf{0}v} \rangle \delta_{vv'} \quad (21)$$

for valence bands and

$$\Delta H_{cc'}^{\text{KI}(2)}(\mathbf{k}) = -\frac{1}{2} \langle n_{\mathbf{q}}^{\mathbf{0}c} | v_{\text{pert},\mathbf{q}}^{\mathbf{0}c} \rangle \delta_{cc'} + \frac{1}{N_{\mathbf{q}}} \sum_{\mathbf{q}} \langle v_{\text{pert},\mathbf{q}}^{\mathbf{0}c'} | n_{\mathbf{k},\mathbf{k}+\mathbf{q}}^{cc'} \rangle \quad (22)$$

for conduction bands, where $n_{\mathbf{k},\mathbf{k}+\mathbf{q}}^{cc'}(\mathbf{r}) = (w_{\mathbf{k}}^c(\mathbf{r}))^* w_{\mathbf{k}+\mathbf{q}}^{c'}(\mathbf{r})$; $w_{\mathbf{k}}^c(r)$ the periodic part of the electronic state in the Wannier gauge. As expected, the KI contribution to the valence bands is \mathbf{k} -independent. The total Hamiltonian is then diagonalized in order to obtain the canonical eigenstates and energies. Given the fact that the Hamiltonian is written in a basis of Wannier functions, it is also possible to employ standard interpolation techniques to obtain the KI eigenvalues at any arbitrary \mathbf{k} -point.⁵⁰

Because all of these equations are formulated in terms of a primitive cell with \mathbf{k} -point sampling, `kcw.x` uses MPI to parallelize over \mathbf{k} -points. It also parallelizes over plane-wave orbitals (as already introduced in the context of `kcp.x`). The fact that `kcw.x` operates in a primitive cell but `kcp.x` operates in a supercell also has implications for how the two algorithms scale. `kcp.x` requires one SCF calculation per orbital, which takes a computational time T^{SC} that roughly scales as $\mathcal{O}\left((N_{\text{el}}^{\text{SC}})^3\right)$, where $N_{\text{el}}^{\text{SC}}$ is the number of electrons in the supercell. The `kcw.x` DFPT approach scales as $T^{\text{PC}} \propto N_{\mathbf{q}} N_{\mathbf{k}} N_{\text{el}}^{\text{PC}3}$. This is the typical computational time for the SCF cycle $N_{\mathbf{k}} N_{\text{el}}^{\text{PC}3}$ times the number of independent monochromatic perturbations $N_{\mathbf{q}}$. Using the relation $N_{\text{el}}^{\text{SC}} = N_{\mathbf{k}} N_{\text{el}}^{\text{PC}}$ and the fact that $N_{\mathbf{q}} = N_{\mathbf{k}}$, the ratio between the supercell and primitive computational times is $T^{\text{SC}}/T^{\text{PC}} \propto N_{\mathbf{q}}$. Thus, as the supercell size (or equivalently the number of \mathbf{q} -points in the primitive cell) increases, the `kcw.x` DFPT approach becomes more and more computationally efficient.⁴⁹

That said, `kcw.x` makes two approximations that `kcp.x` does not: the DFPT approach expands the total energy only to second order when computing screening parameters (see Section 1.3.2), and it does not optimize the variational orbitals. These are instead defined via Wannier functions, which often closely resemble the minimizing orbitals of the Koopmans energy functional. This also means that `kcw.x` only implements the KI functional. Without

orbital minimization one cannot perform KIPZ calculations, and pKIPZ would require the PZ kernel (i.e. the second derivative of the PZ energy with respect to the density), and this is not implemented in common electronic structure codes.

While much of the above applies to periodic systems, `kcw.x` can still be used to perform calculations on aperiodic systems. The Wannier function basis still remains valid, and we can even obtain the full KI contribution rather than only being able to compute it to second order (refer back to Equation 22), but we no longer have multiple \mathbf{k} -points.

In addition to being part of the `koopmans` package, `kcw.x` is part of the official Quantum ESPRESSO distribution (from version 7.1 onward).

4 Conclusions

Koopmans functionals are a powerful computational tool for predicting the spectral properties of materials from first principles at low computational cost. This has already been demonstrated in their ability to calculate the ionization potentials and electron affinities of small molecules,^{39,44} photoemission spectra,^{39,40} the electronic structure of liquid water,⁷⁶ and the band structures and ionization potentials of prototypical semiconductors and insulators,^{41,43,49} all at a level of accuracy comparable to state-of-the-art many-body perturbation methods.

The newly released `koopmans` package now makes it possible, for the first time, for non-experts to use these functionals in their own research. Experts will also benefit from their calculations becoming much more robust and reproducible. For more information, we refer the reader to the website, koopmans-functionals.org.

The `koopmans` package will continue to be maintained and developed. In particular, Koopmans calculations on periodic systems require the user to perform a Wannierization of the electronic states, and correctly configuring this calculation can be onerous. In the near future we will add support for automated Wannierization, using an approach similar to Ref.

77.

The second focus of ongoing development will be parallelism. Large swathes of the `Koopmans` workflow (for example, the calculation of screening parameters) are embarrassingly parallelizable. For example, one could calculate a revised value of the screening parameter for orbital i entirely independently of the calculation of the screening parameter for orbital j . (This is true for both the finite difference and DFPT schemes.) However, `koopmans` performs each calculation in the workflow serially i.e. multiple calculations are not run simultaneously. (N.B. We are not saying that individual calculations must be run on a single core; all the codes support MPI parallelization.) Integration of the workflows within a workflow engine such as AiiDA would allow us to massively reduce the workflows' walltimes.⁷⁸ Integration within AiiDA would come with the added benefit of AiiDA's extensive error detection and recovery functionality. Combined with the automated Wannierization and efficient parallelism, high-throughput studies with `Koopmans` functionals are just around the corner.

Acknowledgement

We gratefully acknowledge financial support from the Swiss National Science Foundation (SNSF – project numbers 179138 and 213082). This research was also supported by the NCCR MARVEL, a National Centre of Competence in Research, funded by the Swiss National Science Foundation (grant number 205602). We also acknowledge support from MaX – MAterials design at the eXascale – a European Centre of Excellence funded by the European Union's program HORIZON-EUROHPC-JU-2021-COE-01 (grant number 101093374). NLN acknowledges support by the Vietnam National Foundation for Science and Technology Development (NAFOSTED) under grant number 103.02-2021.95. ID acknowledges support from the Division of Materials Research of the National Science Foundation through CAREER Award number DMR-1654625.

Supporting Information Available

The Supporting Information contains a derivation of the functional form of Koopmans functionals, a detailed description of the Koopmans workflows, and example output `koopmans` files. All of the input and output files related to this paper can be found on Materials Cloud at [10.24435/materialscloud:9w-sp](https://doi.org/10.24435/materialscloud:9w-sp).

Supporting Information

S1 Derivation of the functional form of Koopmans functionals

The brief derivation of the functional form of Koopmans functionals is as follows: let us assume a functional of the form

$$E^{\text{Koopmans}} = E^{\text{DFT}} + \sum_i \Pi_i \quad (\text{S1})$$

If we take the derivative with respect to the occupancy of the j^{th} variational orbital then we have

$$\eta_j = \left. \frac{dE^{\text{DFT}}}{df_j} \right|_{f_j=f} + \left. \frac{d\Pi_j}{df_j} \right|_{f_j=f} = \langle \varphi_j | \hat{h}^{\text{DFT}}(f) | \varphi_j \rangle + \left. \frac{d\Pi_j}{df_j} \right|_{f_j=f} \quad (\text{S2})$$

where we assumed that the cross-term derivatives $d\Pi_i/df_j$ vanish, and because E^{Koopmans} ought to be linear in f_j , we replaced its derivative with some yet-to-be determined constant η_j . For the second equality we invoked Janak's theorem. f is some number between 0 and 1.

Assuming that the our energy correction Π_j is zero at integer occupancies, is independent of f_i for $i \neq j$, and neglecting for the moment any orbital relaxation as the orbital occupancies change, it follows that

$$\Pi_j^u = - \int_0^{f_j} \langle \varphi_j | \hat{h}^{\text{DFT}}(f) | \varphi_j \rangle df + f_j \eta_j = - (E^{\text{DFT}}[\rho] - E^{\text{DFT}}[\rho - \rho_i]) + f_j \eta_j \quad (\text{S3})$$

where the u superscript denotes the fact that we neglected orbital relaxation, and thus this term is “unscreened”. To account for this screening we must introduce some screening parameters $\{\alpha_i\}$ such that $\Pi_j = \alpha_j \Pi_j^u$. Having done this, we arrive at equation 5, the final result.

S2 The importance of localized orbitals

As introduced in Section 1.2 of the main text, it is important that Koopmans corrections are applied to localized orbitals. The reason for this is as follows: for small molecular systems, the ionization potential theorem is violated, total energy differences yield accurate ionization potentials, eigenvalues underestimate the ionization potential (in the case of semi-local DFT), and we can use this mismatch to determine the appropriate Koopmans correction (as explained in Section 1.3 of the main text). In contrast, in the bulk limit the ionization potential is trivially satisfied, but now *both* total energy differences and the Kohn-Sham eigenvalues underestimate the true ionization potential.^{79–81} (This occurs because the eigenstates are totally delocalized across the infinite system and removing a single electron from such an orbital starts to resemble the derivative of the total energy with respect to the orbital occupancy.) This deprives us of a means of determining appropriate Koopmans corrections. To make matters worse, most self-interaction corrections (including Koopmans corrections) become vanishingly small if they are applied to totally delocalized orbitals (such as the eigenstates of bulk systems). This is where the localized variational orbitals come in. For localized orbitals in bulk systems, the equivalent of the ionization potential theorem is violated once more, and the Koopmans corrections are non-vanishing. Crucially, the total energy differences of DFAs also become accurate because they are computed on localized orbitals. Thus, by applying the Koopmans corrections to the variational orbitals (and not the canonical orbitals) Koopmans corrections are well-defined and non-vanishing in the bulk limit, and yield accurate band structures compared to experiment. See Ref. 41 for more details.)

S3 Details of the Koopmans workflows

This appendix contains a detailed breakdown of the two key Koopmans workflows: one for calculations where the screening parameters are calculated via finite differences (Figure S1), and the other via DFPT (Figure S2)

S3.1 The finite-difference workflow

In this workflow, we calculate screening parameters via the method described in Section 1.3.1 of the main text.

37

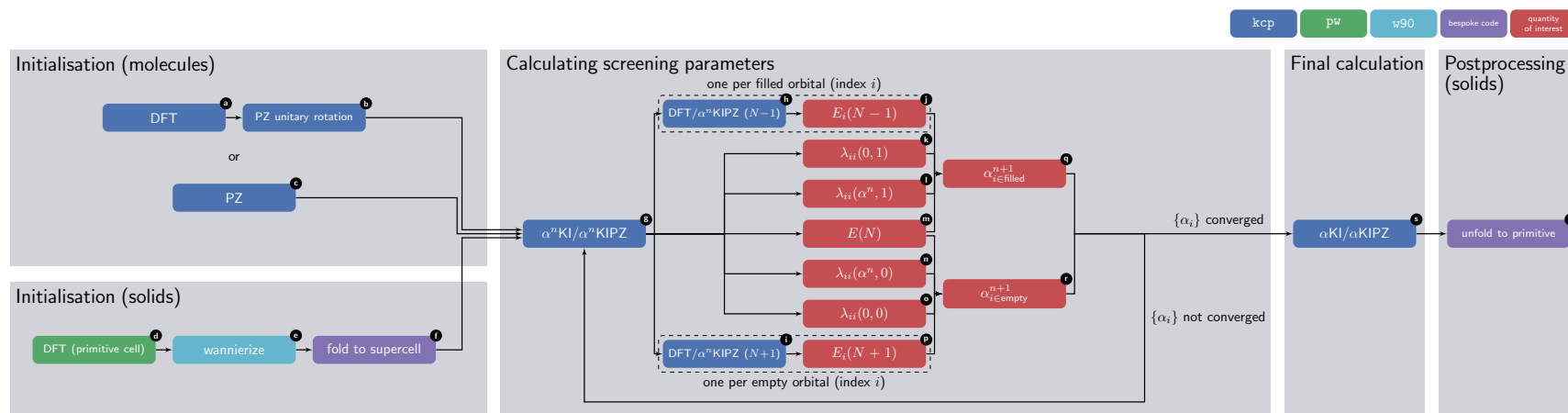


Figure S1: The finite-difference workflow. Individual nodes represent a calculation performed with **QUANTUM ESPRESSO**, except for the red nodes, which represent key quantities of interest that we extract from a preceding calculation. Each individual nodes are explained more fully in the text.

S3.1.1 Initialization

The first step in this workflow is the initialization of the density and the variational orbitals. Depending on the system and functional in question, this can look quite different. For molecules, one can start with a DFT calculation to obtain the ground-state Kohn-Sham eigenvalues (node a in Figure S1). This is typical of KI calculations, which share the same ground-state density as the base DFT functional, in which case the final density has already been determined by this very first calculation. Note, however, that a unitary rotation of the Kohn-Sham orbital densities leaves the total density (and therefore the total energy) unchanged, which means that the variational orbitals from a PBE calculation are not uniquely defined. In order to resolve this issue, one then performs a unitary rotation of the Kohn-Sham variational orbitals minimize the PZ energy (node b). This gives us a unique set of variational orbitals, while leaving the total density unchanged, and fulfils the definition of the KI functional as the $\gamma \rightarrow 0$ limit of the “KI γ PZ” functional (as introduced in Section 1.4.3) in the main text. If one is using the KIPZ functional, it is better to initialize the density and the variational orbitals by performing a full PZ calculation (node c). In contrast to the previous KI approach where the DFT and KI ground-state densities match, the KIPZ and PZ ground-state densities and variational orbitals are similar but not identical, so the PZ solution serves as a suitable initial guess for a KIPZ calculation. Note that all of the above calculations are performed with the Γ -point-only `kcp.x` code.

For solids, the approach for initializing the density and variational orbitals is very different. Here, we take advantage of the periodicity of the lattice by initializing the variational orbitals using maximally localized Wannier functions (MLWFs). This approach is justified by the Wannier-like character of the true minimizing orbitals.⁴³ Practically, the Wannierization procedure involves a DFT calculation with the `pw.x` code (node d), followed by a Wannierization procedure using the `Wannier90` and `pw2wannier90.x` codes (node e).

There are two important points when it comes to the Wannierization. The first is that the occupied and the empty manifolds must be Wannierized separately. This guarantees

that the occupancy matrix is diagonal in the basis of variational orbitals, as required by Koopmans functionals (see Section 1.5 of the main text). The second important point is that mixing bands that are far apart in energy-space is generally detrimental to the Koopmans results. To avoid this, each block of bands that are well-separated in energy-space are Wannierized separately, preventing inter-block mixing during the Wannierization procedure. This is a similar but cruder approach to the so-called dually-localized Wannier functions, where the Wannier functions minimize a localization criteria that is a mix of spatial and energy localization.⁸²

The one final task is to map the Wannier functions in the k -sampled primitive cell to the equivalent Γ -point-only supercell in a format readable by the `kcp.x` code that will handle the subsequent calculation of the screening parameters (node f). In this procedure the supercell dimensions match those of the k -grid used during the initialization.

S3.1.2 Calculating the screening parameters

Having initialized the density and the variational orbitals, the next task to perform is the calculation of the screening parameters. To this end, let us restate equations 8 and 9 from the main text, with which we calculate these parameters:

$$\alpha_i^{n+1} = \alpha_i^n \frac{\Delta E_i - \lambda_{ii}(0, 1)}{\lambda_{ii}(\alpha_i^n, 1) - \lambda_{ii}(0, 1)}; \quad \Delta E_i = E(N) - E_i(N - 1); \quad i \in \text{occupied} \quad (\text{S4})$$

$$\alpha_i^{n+1} = \alpha_i^n \frac{\Delta E_i - \lambda_{ii}(0, 0)}{\lambda_{ii}(\alpha_i^n, 0) - \lambda_{ii}(0, 0)}; \quad \Delta E_i = E_i(N + 1) - E(N); \quad i \in \text{empty} \quad (\text{S5})$$

In order to calculate these screening parameters, we therefore require three calculations. The first calculation is a KI or KIPZ calculation with using a trial screening parameter α^0 (node g). This gives us access to the energy of the N -electron system $E(N)$ (node m) as well as all of the requisite expectation values Koopmans Hamiltonian on the variational orbitals $\lambda_{ii}(\alpha, f)$ (nodes k, l, n, and o). The second and third calculations (nodes h and i) are calculations on the $N \pm 1$ -electron systems, where orbital i is frozen and its occupancy is fixed to 0 (in the

case of occupied orbitals) or 1 (empty orbitals). These calculations yield the total energies $E_i(N \pm 1)$ (nodes j and p). For these calculations in particular, ensuring that there is no spurious interactions between images is crucial (because now we have a charged defect in our system). This requires the use of both a sufficiently large supercell and a correction scheme such as Gygi-Baldereschi.⁷⁵ Note that since KI yields the same total energies as the base functional, these two calculations can be performed at the DFT level when performing the KI workflow.

Having performed these three calculations (nodes g-i) and extracted all of the requisite information (nodes j-p), we can then calculate the screening parameters (nodes q and r) according to the above equations. If the screening parameters are converged, we can then proceed to the final calculation; if not, the process is repeated.

We note that this iterative procedure almost universally converges very quickly. Indeed, for the KI functional and with occupied orbitals, it is guaranteed to converge instantly. This is because, as mentioned earlier, ΔE_i is independent of α , as are occupied variational orbitals, and consequently $\lambda_{ii}^{\text{KI}}(\alpha, 1)$ is linear in α . This is not the case for empty orbitals for the KI functional (for which $\lambda_{ii}^{\text{KI}}(\alpha, 0)$ is not strictly linear) or for the KIPZ functional (where additionally ΔE_i is dependent on α). Even for these functionals, the screening parameters tend to converge in a few iterations.

S3.1.3 The final calculation and postprocessing for solids

We now perform a KI or KIPZ calculation with the finalized set of screening parameters (node s). For a molecular system we are now done: the KI/KIPZ calculation yields a Hamiltonian in the basis of variational orbitals which we diagonalize to extract the quasiparticle energies.

However, for a calculation on a periodic system one final step is required. This is because all of the preceding `kcp.x` calculations have been performed in a Γ -point-only supercell. In order to extract the band structure, we must now unfold the band structure by taking advantage of the MLWF basis, as described in Ref. 43. This step is performed within python

by the `koopmans` workflow manager itself. One trick that we can perform at this stage is “smooth interpolation”. In the supercell, our Hamiltonian in the basis of Wannier functions is given by

$$h_{mn}^{\text{DFT}}(\mathbf{R}) + v_{mn}^{\text{Koopmans}}(\mathbf{R}) \quad (\text{S6})$$

The Koopmans potential is very smooth and slowly-varying in \mathbf{k} -space, applying an almost-constant shift to the Kohn-Sham DFT bands. Consequently, the dominant contribution to the dispersion of the bands comes from the DFT Hamiltonian, and it makes sense to construct the \mathbf{k} -indexed Hamiltonian as

$$h_{mn}(\mathbf{k}) = \sum_{\mathbf{R}'} e^{i\mathbf{k}\cdot\mathbf{R}'} h_{mn}^{\text{DFT}}(\mathbf{R}') + \sum_{\mathbf{R}} e^{i\mathbf{k}\cdot\mathbf{R}} v_{mn}^{\text{Koopmans}}(\mathbf{R}) \quad (\text{S7})$$

where now $\{\mathbf{R}'\}$ corresponds to a much larger supercell or, equivalently, a much denser \mathbf{k} -point grid. The advantage of this strategy is that it improves the interpolation of the band structure at very little computational cost. Suppose we perform a smooth interpolation with a grid twice as fine as the default grid. The only additional computational cost in this instance is having to generate the DFT Hamiltonian in the Wannier basis for this finer grid (i.e. we repeat nodes d and e). This only represents a small fraction of the total workflow, and includes only DFT and not ODDFT calculations, so it only fractionally increases the total computational cost. Contrast this with the alternative, where one could perform the entire calculation with a grid twice as fine. This would require us to perform (among other things) calculations on a supercell containing eight times as many atoms, drastically increasing the computational cost of the workflow as a whole. For more details on the smooth interpolation procedure, refer to Ref. 43.

S3.2 The DFPT workflow

The DFPT workflow is depicted in Figure S2. It is simpler than the finite-difference procedure, because orbital relaxation is not implemented, and instead Wannier functions are

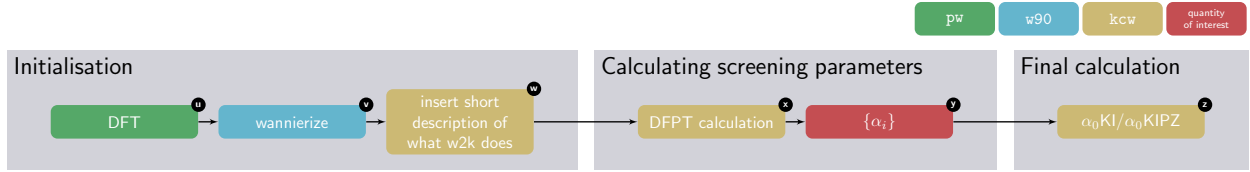


Figure S2: The DFPT workflow. Individual nodes are explained in the text.

used as approximations to the true variational orbitals. This means that only the KI and pKIPZ functionals can be used in this scheme, means that the screening parameters do not need to be calculated self-consistently, and makes the Koopmans functional effectively a post-processing step on top of a DFT calculation.

S3.2.1 Initialization

The initialization procedure for the DFPT workflow is very similar to that for solids in the finite-difference workflow. A primitive cell calculation `pw.x` calculation (node u) is followed by a Wannierization procedure in order to define the density and the variational orbitals (node v). The one difference is that now, instead of using `kpw.x` to map these Wannier functions to a supercell that is readable by `kcp.x`, we use `kpw.x` to convert the Wannier functions to more convenient format for subsequent calculations (node w). Note that `kpw.x` does not map to a supercell because this workflow operates entirely within the primitive cell with k -point sampling.

S3.2.2 Calculating the screening parameters

DFPT calculations evaluating equation 10 (from the main text) are then performed by a single `kpw.x` run (node x). These calculations yield the screening parameters (node y).

S3.2.3 The final calculation and postprocessing for solids

Having calculated the screening parameters, the Koopmans Hamiltonian is constructed in the basis of Wannier functions and then diagonalized, resulting in the full band structure of the system at hand (node z). Like the previous calculations, this is performed using `kpw.x`.

S4 Example output files

All of the input and output files related to this paper can be found on Materials Cloud at [10.24435/materialscloud:9w-sp](https://materialscloud.org/10.24435/materialscloud:9w-sp). We include below a few output files for convenience.

S4.1 Ozone

The output of `koopmans ozone.json`, which prompts a sequence of Quantum ESPRESSO calculations necessary to initialize the density and variational orbitals (lines 16-22), calculate the screening parameters (lines 24-68), and run a final KI calculation (lines 85-87).

```
1  _
2  | | _ _ _ _ _ _ _ _ _ _ _ _ _ _ _ _ _ _ _ _ _ _ _ _ _ _ _ _ _ _ _ _ _ _
3  | | / / _ \ / _ \ | ' _ \ | ' _ \ _ \ / _ \ | ' _ \ \ _ _ |
4  | | < ( ) | ( ) | | ) | | | | | | ( | | | | \ _ _ \
5  | | \ \ _ _ / \ _ _ / | . _ _ / | | | | | \ _ _ , | | | | _ _ /
6  | |
7
8  Koopmans spectral functional calculations with Quantum ESPRESSO
...
16  Initialization of density and variational orbitals
17  =====
18  Running init/dft_init_nspin1... done
19  Running init/dft_init_nspin2_dummy... done
20  Running init/dft_init_nspin2... done
21  Overwriting the variational orbitals with Kohn-Sham orbitals
22  Copying the spin-up variational orbitals over to the spin-down channel
23
24  Calculating screening parameters
25  =====
26
27  SC iteration 1
28  -----
29  Running calc_alpha/iteration_1/ki... done
30
31  Orbital 1
32  -----
33  Running calc_alpha/iteration_1/orbital_1/dft_n-1... done
34
...
67  Orbital 10
68  -----
```

```

69 Running calc_alpha/iteration_1/orbital_10/pz_print... done
70 Running calc_alpha/iteration_1/orbital_10/dft_n+1_dummy... done
71 Running calc_alpha/iteration_1/orbital_10/dft_n+1... done
72
...
87 SC iteration 2
88 -----
89 Running calc_alpha/iteration_2/ki_nspin1_dummy... done
90 Running calc_alpha/iteration_2/ki_nspin1... done
91 Running calc_alpha/iteration_2/ki_nspin2_dummy... done
92 Running calc_alpha/iteration_2/ki_nspin2... done
93
94 Orbital 10
95 -----
96 Running calc_alpha/iteration_2/orbital_10/pz_print... done
97 Running calc_alpha/iteration_2/orbital_10/dft_n+1_dummy... done
98 Running calc_alpha/iteration_2/orbital_10/dft_n+1... done
99
100 alpha
101      1      2      3      4      ...      7      8      9      10
102 0 0.600000 0.600000 0.600000 0.600000 ... 0.600000 0.6000 0.600000 0.600000
103 1 0.655689 0.727571 0.783859 0.66386 ... 0.729888 0.7419 0.779264 0.717389
104 2 0.655689 0.727571 0.783859 0.66386 ... 0.729888 0.7419 0.779264 0.717389
105
...
115 Screening parameters have been converged
116
117 Final KI calculation
118 =====
119 Running final/ki_final... done
120
121 Workflow complete

```

S4.2 Silicon

The output of `koopmans si.json`, which prompts a sequence of Quantum ESPRESSO calculations necessary to initialize the density and variational orbitals using Wannier functions (lines 20-29), fold these k -resolved functions to the equivalent Γ -only supercell (lines 31-36) calculate the screening parameters (lines 38-73), run a final KI calculation (lines 75-77), and finally perform a second DFT Wannierization on a finer k -grid to produce a smoothly interpolated band structure (lines 80-97).


```

59
60 alpha
61      1      2      3      ...      510      511      512
62 0 0.100000 0.100000 0.100000 ... 0.100000 0.100000 0.100000
63 1 0.104648 0.104648 0.104648 ... 0.047709 0.047709 0.047709
64
65 [2 rows x 512 columns]
66
67 Delta E_i - epsilon_i (eV)
68      1      2      3      ...      510      511      512
69 0 -0.023309 -0.023309 -0.023309 ... -0.139624 -0.139624 -0.139624
70
71 [1 rows x 512 columns]
72
73 Screening parameters have been determined but are not necessarily converged
74
75 Final KI calculation
76 =====
77 Running final/ki_final... done
78
79
80 Postprocessing
81 =====
82
83 Wannierization
84 =====
85 Running wannier/scf... done
86 Running wannier/nscf... done
87 Running wannier/block_1/wann_preproc... done
88 Running wannier/block_1/pw2wan... done
89 Running wannier/block_1/wann... done
90 Running wannier/block_2/wann_preproc... done
91 Running wannier/block_2/pw2wan... done
92 Running wannier/block_2/wann... done
93 Running wannier/bands... done
94 UserWarning: Some of the pseudopotentials do not have PP_PSWFC blocks, which means a
↳ projected DOS calculation is not possible. Skipping...
95 Running occ/ki... done
96 Running emp/ki... done
97 UserWarning: The DOS will not be plotted, because the Brillouin zone is too poorly
↳ sampled for the specified value of smearing. In order to generate a DOS, increase the
↳ k-point density ("kpath_density" in the "setup" "k_points" subblock) and/or the
↳ smearing ("degauss" in the "plot" block)
98
99 Workflow complete

```



```
45
46 Calculation of screening parameters
47 =====
48 Running screening/band_2/kc... done
49 Running screening/band_6/kc... done
50 Running screening/band_8/kc... done
51 Running screening/band_10/kc... done
52 Running screening/band_16/kc... done
53 Running screening/band_18/kc... done
54 Running screening/band_20/kc... done
55 Running screening/band_24/kc... done
56 Running screening/band_26/kc... done
57 Running screening/band_27/kc... done
58
59 Regular grid calculations
60 =====
61
62 Wannierization
63 =====
64 Running wannier/scf... done
65 Running wannier/nscf... done
66 Running wannier/block_1/wann_preproc... done
67 Running wannier/block_1/pw2wan... done
68 Running wannier/block_1/wann... done
69 Running wannier/block_2/wann_preproc... done
70 Running wannier/block_2/pw2wan... done
71 Running wannier/block_2/wann... done
72 Running wannier/block_3/wann_preproc... done
73 Running wannier/block_3/pw2wan... done
74 Running wannier/block_3/wann... done
75 Running wannier/block_4/wann_preproc... done
76 Running wannier/block_4/pw2wan... done
77 Running wannier/block_4/wann... done
78 Running wannier/block_5/wann_preproc... done
79 Running wannier/block_5/pw2wan... done
80 Running wannier/block_5/wann... done
81 Running wannier/bands... done
82 Running pdos/projwfc... done
83
84 Conversion to Koopmans format
85 -----
86 Running wannier/kc... done
87
88 Construction of the Hamiltonian
89 =====
90 Running hamiltonian/kc... done
91
92 Workflow complete
```

References

- (1) Hedin, L. New Method for Calculating the One-Particle Green's Function with Application to the Electron-Gas Problem. *Phys. Rev.* **1965**, *139*, A796–A823.
- (2) Aryasetiawan, F.; Gunnarsson, O. The GW Method. *Rep. Prog. Phys.* **1998**, *61*, 237–312.
- (3) Foulkes, W. M. C.; Mitas, L.; Needs, R. J.; Rajagopal, G. Quantum Monte Carlo Simulations of Solids. *Rev. Mod. Phys.* **2001**, *73*, 33–83.
- (4) Stanton, J. F.; Bartlett, R. J. The Equation of Motion Coupled-cluster Method. A Systematic Biorthogonal Approach to Molecular Excitation Energies, Transition Probabilities, and Excited State Properties. *J. Chem. Phys.* **1993**, *98*, 7029–7039.
- (5) Golze, D.; Dvorak, M.; Rinke, P. The GW Compendium: A Practical Guide to Theoretical Photoemission Spectroscopy. *Front. Chem.* **2019**, *7*.
- (6) van Setten, M. J.; Giantomassi, M.; Bousquet, E.; Verstraete, M. J.; Hamann, D. R.; Gonze, X.; Rignanese, G. M. The PseudoDojo: Training and Grading a 85 Element Optimized Norm-Conserving Pseudopotential Table. *Computer Physics Communications* **2018**, *226*, 39–54.
- (7) Bonacci, M.; Qiao, J.; Spallanzani, N.; Marrazzo, A.; Pizzi, G.; Molinari, E.; Varsano, D.; Ferretti, A.; Prezzi, D. Towards High-Throughput Many-Body Perturbation Theory: Efficient Algorithms and Automated Workflows. 2023.
- (8) Bruneval, F.; Dattani, N.; van Setten, M. J. The GW Miracle in Many-Body Perturbation Theory for the Ionization Potential of Molecules. *Front. Chem.* **2021**, *9*, 811.
- (9) Hohenberg, P.; Kohn, W. Inhomogeneous Electron Gas. *Phys. Rev.* **1964**, *136*, B864–B871.

- (10) Kohn, W.; Sham, L. J. Self-Consistent Equations Including Exchange and Correlation Effects. *Phys. Rev.* **1965**, *140*, A1133–A1138.
- (11) Almladh, C.-O.; von Barth, U. Exact Results for the Charge and Spin Densities, Exchange-Correlation Potentials, and Density-Functional Eigenvalues. *Phys. Rev. B* **1985**, *31*, 3231–3244.
- (12) Casida, M. E. Generalization of the Optimized-Effective-Potential Model to Include Electron Correlation: A Variational Derivation of the Sham-Schlüter Equation for the Exact Exchange-Correlation Potential. *Phys. Rev. A* **1995**, *51*, 2005–2013.
- (13) Cohen, A. J.; Mori-Sánchez, P.; Yang, W. Fractional Charge Perspective on the Band Gap in Density-Functional Theory. *Phys. Rev. B* **2008**, *77*.
- (14) Anisimov, V. I.; Zaanen, J.; Andersen, O. K. Band Theory and Mott Insulators: Hubbard U Instead of Stoner I. *Phys. Rev. B* **1991**, *44*, 943–954.
- (15) Cococcioni, M.; de Gironcoli, S. Linear Response Approach to the Calculation of the Effective Interaction Parameters in the LDA + U Method. *Phys. Rev. B* **2005**, *71*, 035105.
- (16) Perdew, J. P.; Ernzerhof, M.; Burke, K. Rationale for Mixing Exact Exchange with Density Functional Approximations. *J. Chem. Phys.* **1996**, *105*, 9982–9985.
- (17) Marsman, M.; Paier, J.; Stroppa, A.; Kresse, G. Hybrid Functionals Applied to Extended Systems. *J. Phys. Condens. Matter* **2008**, *20*, 064201.
- (18) Sai, N.; Barbara, P. F.; Leung, K. Hole Localization in Molecular Crystals from Hybrid Density Functional Theory. *Phys. Rev. Lett.* **2011**, *106*, 226403.
- (19) Atalla, V.; Zhang, I. Y.; Hofmann, O. T.; Ren, X.; Rinke, P.; Scheffler, M. Enforcing the Linear Behavior of the Total Energy with Hybrid Functionals: Implications for

- Charge Transfer, Interaction Energies, and the Random-Phase Approximation. *Phys. Rev. B* **2016**, *94*, 035140.
- (20) Kronik, L.; Stein, T.; Refaely-Abramson, S.; Baer, R. Excitation Gaps of Finite-Sized Systems from Optimally Tuned Range-Separated Hybrid Functionals. *J. Chem. Theory Comput.* **2012**, *8*, 1515–1531.
- (21) Brawand, N. P.; Vörös, M.; Govoni, M.; Galli, G. Generalization of Dielectric-Dependent Hybrid Functionals to Finite Systems. *Phys. Rev. X* **2016**, *6*, 041002.
- (22) Chen, W.; Miceli, G.; Rignanese, G.-M.; Pasquarello, A. Nonempirical Dielectric-Dependent Hybrid Functional with Range Separation for Semiconductors and Insulators. *Phys. Rev. Materials* **2018**, *2*, 073803.
- (23) Miceli, G.; Chen, W.; Reshetnyak, I.; Pasquarello, A. Nonempirical Hybrid Functionals for Band Gaps and Polaronic Distortions in Solids. *Phys. Rev. B* **2018**, *97*, 121112.
- (24) Skone, J. H.; Govoni, M.; Galli, G. Nonempirical Range-Separated Hybrid Functionals for Solids and Molecules. *Phys. Rev. B* **2016**, *93*, 235106.
- (25) Wing, D.; Ohad, G.; Haber, J. B.; Filip, M. R.; Gant, S. E.; Neaton, J. B.; Kronik, L. Band Gaps of Crystalline Solids from Wannier-localization–Based Optimal Tuning of a Screened Range-Separated Hybrid Functional. *Proc. Natl. Acad. Sci.* **2021**, *118*, e2104556118.
- (26) Ma, J.; Wang, L.-W. Using Wannier Functions to Improve Solid Band Gap Predictions in Density Functional Theory. *Sci. Rep.* **2016**, *6*, 24924.
- (27) Li, C.; Zheng, X.; Su, N. Q.; Yang, W. Localized Orbital Scaling Correction for Systematic Elimination of Delocalization Error in Density Functional Approximations. *Natl. Sci. Rev.* **2018**, *5*, 203–215.

- (28) Yang, X.; Zheng, X.; Yang, W. Density Functional Prediction of Quasiparticle, Excitation, and Resonance Energies of Molecules With a Global Scaling Correction Approach. *Front. Chem.* **2020**, *8*, 979.
- (29) Mei, Y.; Yu, J.; Chen, Z.; Su, N. Q.; Yang, W. LibSC: Library for Scaling Correction Methods in Density Functional Theory. *J. Chem. Theory Comput.* **2022**, *18*, 840–850.
- (30) Valone, S. M. A One-to-one Mapping between One-particle Densities and Some N-particle Ensembles. *J. Chem. Phys.* **1980**, *73*, 4653–4655.
- (31) Baerends, E. J. Chemical Potential, Derivative Discontinuity, Fractional Electrons, Jump of the Kohn-Sham Potential, Atoms as Thermodynamic Open Systems, and Other (Mis)Conceptions of the Density Functional Theory of Electrons in Molecules. 2022.
- (32) Kirkpatrick, J.; McMorrow, B.; Turban, D. H. P.; Gaunt, A. L.; Spencer, J. S.; Matthews, A. G. D. G.; Obika, A.; Thiry, L.; Fortunato, M.; Pfau, D.; Castellanos, L. R.; Petersen, S.; Nelson, A. W. R.; Kohli, P.; Mori-Sánchez, P.; Hassabis, D.; Cohen, A. J. Pushing the Frontiers of Density Functionals by Solving the Fractional Electron Problem. *Science* **2021**, *374*, 1385–1389.
- (33) Dabo, I.; Cococcioni, M.; Marzari, N. Non-Koopmans Corrections in Density-functional Theory: Self-interaction Revisited. 2009; <http://arxiv.org/abs/0901.2637>.
- (34) Dabo, I.; Ferretti, A.; Poilvert, N.; Li, Y.; Marzari, N.; Cococcioni, M. Koopmans' Condition for Density-Functional Theory. *Phys. Rev. B* **2010**, *82*, 115121.
- (35) Dabo, I.; Ferretti, A.; Park, C. H.; Poilvert, N.; Li, Y.; Cococcioni, M.; Marzari, N. Donor and Acceptor Levels of Organic Photovoltaic Compounds from First Principles. *Phys. Chem. Chem. Phys.* **2013**, *15*, 685–695.

- (36) Borghi, G.; Ferretti, A.; Nguyen, N. L.; Dabo, I.; Marzari, N. Koopmans-Compliant Functionals and Their Performance against Reference Molecular Data. *Phys. Rev. B* **2014**, *90*, 075135.
- (37) Ferretti, A.; Dabo, I.; Cococcioni, M.; Marzari, N. Bridging Density-Functional and Many-Body Perturbation Theory: Orbital-Density Dependence in Electronic-Structure Functionals. *Phys. Rev. B* **2014**, *89*, 195134.
- (38) Borghi, G.; Park, C. H.; Nguyen, N. L.; Ferretti, A.; Marzari, N. Variational Minimization of Orbital-Density-Dependent Functionals. *Phys. Rev. B* **2015**, *91*, 155112.
- (39) Nguyen, N. L.; Borghi, G.; Ferretti, A.; Dabo, I.; Marzari, N. First-Principles Photoemission Spectroscopy and Orbital Tomography in Molecules from Koopmans-Compliant Functionals. *Phys. Rev. Lett.* **2015**, *114*, 166405.
- (40) Nguyen, N. L.; Borghi, G.; Ferretti, A.; Marzari, N. First-Principles Photoemission Spectroscopy of DNA and RNA Nucleobases from Koopmans-Compliant Functionals. *J. Chem. Theory Comput.* **2016**, *12*, 3948–3958.
- (41) Nguyen, N. L.; Colonna, N.; Ferretti, A.; Marzari, N. Koopmans-Compliant Spectral Functionals for Extended Systems. *Phys. Rev. X* **2018**, *8*, 021051.
- (42) Colonna, N.; Nguyen, N. L.; Ferretti, A.; Marzari, N. Screening in Orbital-Density-Dependent Functionals. *J. Chem. Theory Comput.* **2018**, *14*, 2549–2557.
- (43) De Gennaro, R.; Colonna, N.; Linscott, E.; Marzari, N. Bloch’s Theorem in Orbital-Density-Dependent Functionals: Band Structures from Koopmans Spectral Functionals. *Phys. Rev. B* **2022**, *106*, 035106.
- (44) Colonna, N.; Nguyen, N. L.; Ferretti, A.; Marzari, N. Koopmans-Compliant Functionals and Potentials and Their Application to the GW100 Test Set. *J. Chem. Theory Comput.* **2019**, *15*, 1905–1914.

- (45) Schubert, Y.; Marzari, N.; Linscott, E. Testing Koopmans Spectral Functionals on the Analytically-Solvable Hooke’s Atom. 2022; <https://arxiv.org/abs/2212.05950>.
- (46) Perdew, J. P.; Parr, R. G.; Levy, M.; Balduz, J. L. Density-Functional Theory for Fractional Particle Number: Derivative Discontinuities of the Energy. *Phys. Rev. Lett.* **1982**, *49*, 1691–1694.
- (47) Gatti, M.; Olevano, V.; Reining, L.; Tokatly, I. V. Transforming Nonlocality into a Frequency Dependence: A Shortcut to Spectroscopy. *Phys. Rev. Lett.* **2007**, *99*, 057401.
- (48) Baroni, S.; de Gironcoli, S.; Dal Corso, A.; Giannozzi, P. Phonons and Related Crystal Properties from Density-Functional Perturbation Theory. *Rev. Mod. Phys.* **2001**, *73*, 515–562.
- (49) Colonna, N.; Gennaro, R. D.; Linscott, E.; Marzari, N. Koopmans Spectral Functionals in Periodic Boundary Conditions. *J. Chem. Theory Comput.* **2022**,
- (50) Marzari, N.; Mostofi, A. A.; Yates, J. R.; Souza, I.; Vanderbilt, D. Maximally Localized Wannier Functions: Theory and Applications. *Rev. Mod. Phys.* **2012**, *84*, 1419–1475.
- (51) Van Setten, M. J.; Caruso, F.; Sharifzadeh, S.; Ren, X.; Scheffler, M.; Liu, F.; Lischner, J.; Lin, L.; Deslippe, J. R.; Louie, S. G.; Yang, C.; Weigend, F.; Neaton, J. B.; Evers, F.; Rinke, P. GW100: Benchmarking G0W0 for Molecular Systems. *J. Chem. Theory Comput.* **2015**, *11*, 5665–5687.
- (52) Caruso, F.; Dauth, M.; van Setten, M. J.; Rinke, P. Benchmark of GW Approaches for the GW 100 Test Set. *J. Chem. Theory Comput.* **2016**, *12*, 5076–5087.
- (53) Krause, K.; Harding, M. E.; Klopper, W. Coupled-Cluster Reference Values for the GW27 and GW100 Test Sets for the Assessment of GW Methods. *Mol. Phys.* **2015**, *113*, 1952–1960.

- (54) Linstrom, P.; Mallard, W. *NIST Chemistry WebBook, NIST Standard Reference Database Number 69*; National Institute of Standards and Technology: Gaithersburg MD, 20899.
- (55) Katsumata, S.; Shiromaru, H.; Kimura, T. Photoelectron Angular Distribution and Assignment of Photoelectron Spectrum of Ozone. *BCSJ* **1984**, *57*, 1784–1788.
- (56) Novich, S. E.; Engelking, P. C.; Jones, P. L.; Futrell, J. H.; Lineberger, W. C. Laser Photoelectron, Photodetachment, and Photodestruction Spectra of O₃⁻. *J. Chem. Phys.* **1979**, *70*, 2652.
- (57) Arnold, D. W.; Xu, C. S.; Kim, E. H.; Neumark, D. M. Study of Low-Lying Electronic States of Ozone by Anion Photoelectron Spectroscopy of O₃⁻. *J. Chem. Phys.* **1994**, *101*, 912.
- (58) Shishkin, M.; Kresse, G. Self-Consistent GW Calculations for Semiconductors and Insulators. *Phys. Rev. B* **2007**, *75*, 235102.
- (59) Shishkin, M.; Marsman, M.; Kresse, G. Accurate Quasiparticle Spectra from Self-Consistent GW Calculations with Vertex Corrections. *Phys. Rev. Lett.* **2007**, *99*, 246403.
- (60) Madelung, O. *Semiconductors*, 3rd ed.; Springer-Verlag: Berlin, 2004.
- (61) Miglio, A.; Brousseau-Couture, V.; Godbout, E.; Antonius, G.; Chan, Y.-H.; Louie, S. G.; Côté, M.; Giantomassi, M.; Gonze, X. Predominance of Non-Adiabatic Effects in Zero-Point Renormalization of the Electronic Band Gap. *npj Comput Mater* **2020**, *6*, 1–8.
- (62) Kittel, C. *Introduction to Solid State Physics*, 8th ed.; Wiley: Hoboken, NJ, 2004.

- (63) Manjón, F. J.; Mollar, M.; Hernández-Fenollosa, M. A.; Marí, B.; Lauck, R.; Cardona, M. Effect of Isotopic Mass on the Photoluminescence Spectra of Zinc Oxide. *Solid State Communications* **2003**, *128*, 35–39.
- (64) Giannozzi, P.; Baroni, S.; Bonini, N.; Calandra, M.; Car, R.; Cavazzoni, C.; Ceresoli, D.; Chiarotti, G. L.; Cococcioni, M.; Dabo, I.; Dal Corso, A.; de Gironcoli, S.; Fabris, S.; Fratesi, G.; Gebauer, R.; Gerstmann, U.; Gougoussis, C.; Kokalj, A.; Lazzeri, M.; Martin-Samos, L.; Marzari, N.; Mauri, F.; Mazzarello, R.; Paolini, S.; Pasquarello, A.; Paulatto, L.; Sbraccia, C.; Scandolo, S.; Sclauzero, G.; Seitsonen, A. P.; Smogunov, A.; Umari, P.; Wentzcovitch, R. M. QUANTUM ESPRESSO: A Modular and Open-Source Software Project for Quantum Simulations of Materials. *J. Phys. Condens. Matter* **2009**, *21*, 395502.
- (65) Giannozzi, P.; Andreussi, O.; Brumme, T.; Bunau, O.; Buongiorno Nardelli, M.; Calandra, M.; Car, R.; Cavazzoni, C.; Ceresoli, D.; Cococcioni, M.; Colonna, N.; Carnimeo, I.; Dal Corso, A.; de Gironcoli, S.; Delugas, P.; DiStasio, R. A.; Ferretti, A.; Floris, A.; Fratesi, G.; Fugallo, G.; Gebauer, R.; Gerstmann, U.; Giustino, F.; Gorni, T.; Jia, J.; Kawamura, M.; Ko, H.-Y.; Kokalj, A.; Küçükbenli, E.; Lazzeri, M.; Marsili, M.; Marzari, N.; Mauri, F.; Nguyen, N. L.; Nguyen, H.-V.; Otero-de-la-Roza, A.; Paulatto, L.; Poncé, S.; Rocca, D.; Sabatini, R.; Santra, B.; Schlipf, M.; Seitsonen, A. P.; Smogunov, A.; Timrov, I.; Thonhauser, T.; Umari, P.; Vast, N.; Wu, X.; Baroni, S. Advanced Capabilities for Materials Modelling with Quantum ESPRESSO. *J. Phys. Condens. Matter* **2017**, *29*, 465901.
- (66) Larsen, A. H.; Mortensen, J. J.; Blomqvist, J.; Castelli, I. E.; Christensen, R.; Dułak, M.; Friis, J.; Groves, M. N.; Hammer, B.; Hargus, C.; Hermes, E. D.; Jennings, P. C.; Bjerre Jensen, P.; Kermode, J.; Kitchin, J. R.; Leonhard Kolsbjerg, E.; Kubal, J.; Kaasbjerg, K.; Lysgaard, S.; Maronsson, J. B.; Maxson, T.; Olsen, T.; Pastewka, L.; Peterson, A.; Rostgaard, C.; Schiøtz, J.; Schütt, O.; Strange, M.; Thyge-

- sen, K. S.; Vegge, T.; Vilhelmsen, L.; Walter, M.; Zeng, Z.; Jacobsen, K. W. The Atomic Simulation Environment—a Python Library for Working with Atoms. *J. Phys. Condens. Matter* **2017**, *29*, 273002.
- (67) Krekel, H.; Oliveira, B.; Pfannschmidt, R.; Bruynooghe, F.; Laughner, B.; Bruhin, F. Pytest 7.1. 2004; <https://github.com/pytest-dev/pytest>.
- (68) Pizzi, G.; Vitale, V.; Arita, R.; Blügel, S.; Freimuth, F.; Géranton, G.; Gibertini, M.; Gresch, D.; Johnson, C.; Koretsune, T.; Ibañez-Azpiroz, J.; Lee, H.; Lihm, J.-M.; Marchand, D.; Marrazzo, A.; Mokrousov, Y.; Mustafa, J. I.; Nohara, Y.; Nomura, Y.; Paulatto, L.; Poncé, S.; Ponweiser, T.; Qiao, J.; Thöle, F.; Tsirkin, S. S.; Wierzbowska, M.; Marzari, N.; Vanderbilt, D.; Souza, I.; Mostofi, A. A.; Yates, J. R. Wannier90 as a Community Code: New Features and Applications. *J. Phys.: Condens. Matter* **2020**, *32*, 165902.
- (69) Marzari, N.; Vanderbilt, D.; Payne, M. C. Ensemble Density-Functional Theory for Ab Initio Molecular Dynamics of Metals and Finite-Temperature Insulators. *Phys. Rev. Lett.* **1997**, *79*, 1337–1340.
- (70) Klüpfel, S.; Klüpfel, P.; Jónsson, H. Importance of Complex Orbitals in Calculating the Self-Interaction-Corrected Ground State of Atoms. *Phys. Rev. A* **2011**, *84*, 050501.
- (71) Hofmann, D.; Klüpfel, S.; Klüpfel, P.; Kümmel, S. Using Complex Degrees of Freedom in the Kohn-Sham Self-Interaction Correction. *Phys. Rev. A* **2012**, *85*, 062514.
- (72) Lehtola, S.; Jónsson, H. Variational, Self-Consistent Implementation of the Perdew–Zunger Self-Interaction Correction with Complex Optimal Orbitals. *J. Chem. Theory Comput.* **2014**, *10*, 5324–5337.
- (73) Lehtola, S.; Head-Gordon, M.; Jónsson, H. Complex Orbitals, Multiple Local Minima, and Symmetry Breaking in Perdew–Zunger Self-Interaction Corrected Density Functional Theory Calculations. *J. Chem. Theory Comput.* **2016**, *12*, 3195–3207.

- (74) Martyna, G. J.; Tuckerman, M. E. A Reciprocal Space Based Method for Treating Long Range Interactions in Ab Initio and Force-Field-Based Calculations in Clusters. *J. Chem. Phys.* **1999**, *110*, 2810.
- (75) Gygi, F.; Baldereschi, A. Self-Consistent Hartree-Fock and Screened-Exchange Calculations in Solids: Application to Silicon. *Phys. Rev. B* **1986**, *34*, 4405–4408.
- (76) de Almeida, J. M.; Nguyen, N. L.; Colonna, N.; Chen, W.; Rodrigues Miranda, C.; Pasquarello, A.; Marzari, N. Electronic Structure of Water from Koopmans-Compliant Functionals. *J. Chem. Theory Comput.* **2021**, *17*, 3923–3930.
- (77) Vitale, V.; Pizzi, G.; Marrazzo, A.; Yates, J. R.; Marzari, N.; Mostofi, A. A. Automated High-Throughput Wannierisation. *npj Comput Mater* **2020**, *6*, 1–18.
- (78) Huber, S. P.; Zoupanos, S.; Uhrin, M.; Talirz, L.; Kahle, L.; Häuselmann, R.; Gresch, D.; Müller, T.; Yakutovich, A. V.; Andersen, C. W.; Ramirez, F. F.; Adorf, C. S.; Gargiulo, F.; Kumbhar, S.; Passaro, E.; Johnston, C.; Merkys, A.; Cepellotti, A.; Mounet, N.; Marzari, N.; Kozinsky, B.; Pizzi, G. AiiDA 1.0, a Scalable Computational Infrastructure for Automated Reproducible Workflows and Data Provenance. *Sci Data* **2020**, *7*, 300.
- (79) Mori-Sánchez, P.; Cohen, A. J.; Yang, W. Localization and Delocalization Errors in Density Functional Theory and Implications for Band-Gap Prediction. *Phys. Rev. Lett.* **2008**, *100*, 146401.
- (80) Kraisler, E.; Kronik, L. Fundamental Gaps with Approximate Density Functionals: The Derivative Discontinuity Revealed from Ensemble Considerations. *J. Chem. Phys.* **2014**, *140*, 18A540.
- (81) Vlček, V.; Eisenberg, H. R.; Steinle-Neumann, G.; Kronik, L.; Baer, R. Deviations from Piecewise Linearity in the Solid-State Limit with Approximate Density Functionals. *J. Chem. Phys.* **2015**, *142*, 034107.

(82) Mahler, A.; Williams, J. Z.; Su, N. Q.; Yang, W. Wannier Functions Dually Localized in Space and Energy. *ArXiv220107751 Cond-Mat* **2022**,

Graphical TOC Entry

